

**TOWARDS PRODUCING PHOTON TRIPLETS
VIA SIX-WAVE MIXING IN RUBIDIUM-87**

RITTIK MITRA

**ENGINEERING SCIENCE PROGRAMME
NATIONAL UNIVERSITY OF SINGAPORE**

2021/2022

**TOWARDS PRODUCING PHOTON TRIPLETS
VIA SIX-WAVE MIXING IN RUBIDIUM-87**

RITTIK MITRA

A THESIS SUBMITTED

FOR THE DEGREE OF BACHELOR OF ENGINEERING

ENGINEERING SCIENCE PROGRAMME

NATIONAL UNIVERSITY OF SINGAPORE

Acknowledgement

I would like to thank the members of the Quantum Optics Group for hosting me in their lab during this internship, with special thanks to Professor Christian Kurtsiefer, Dr Tan Peng Kian and Yeo Xi Jie for their invaluable help, mentorship, and guidance through this FYP. I would also like to thank the Engineering Science Program for providing me with the opportunity to embark on this FYP at the Centre for Quantum Technologies, where I have been able to learn so much from so many amazing people.

Abstract

Photon triplet generation is a field being studied for its various potential applications in fields such as quantum cryptography. There are existing methods of producing photon triplets such as cascaded SPDC and third order SPDC (TOSPDC). These methods generate photons with bandwidths on the order of THz or higher, and as such due to bandwidth mismatch they are unsuitable for applications involving light-atom interactions with atomic linewidths being on the order of THz. A proposed scheme for six-wave mixing using Rubidium-87 is postulated to produce narrow-bandwidth photon triplets matching atomic linewidths allowing such a source to be usable for light-atom interaction-based applications. This thesis investigates possible methods and the feasibility of extracting a photon triplet from this six-wave mixing scheme using filtering techniques.

Towards producing photon triplets via six-wave mixing in ^{87}Rb

Rittik Mitra, Undergraduate, Centre for Quantum Technologies

Abstract—Photon triplet generation is a field being studied for its various potential applications in fields such as quantum cryptography. There are existing methods of producing photon triplets such as cascaded SPDC and third order SPDC (TOSPDC). These methods generate photons with bandwidths on the order of THz or higher, and as such due to bandwidth mismatch they are unsuitable for applications involving light-atom interactions with atomic linewidths being on the order of THz. A proposed scheme for six-wave mixing using Rubidium-87 is postulated to produce narrow-bandwidth photon triplets matching atomic linewidths, and hence this report investigates the feasibility of extracting a photon triplet from this six-wave mixing scheme using filtering techniques.

Index Terms—Photon Triplets, Rubidium Spectroscopy, Six-Wave Mixing, External Cavity Laser Diodes, Pound-Drever Hall Locking, Fabry-Perot Cavity

I. Entanglement and Photon pairs

A photon triplet is a group of three photons produced from the same source, which in the context of quantum optics means that they have the property of being time correlated. There are various methods by which photon triplets can be generated[1]–[5], such as Third order SPDC, a process where a single photon is converted into three photons, or cascaded SPDC, a two-step cascaded photon-pair production process where a photon is split into a photon pair where one of the generated photons undergoes this process again to produce another photon pair forming a photon triplet[6].

In Spontaneous Parametric Down Conversion (SPDC), the production of photon pairs is described by the second order susceptibility $\chi^{(2)}$ of a non-linear crystal. This process was first observed in [7] and has been the most widely used means of producing correlated photon pairs for the past few decades. This process allows for photon pairs to be produced in well-defined spatial modes, but with a broad bandwidth ranging from 0.1 to 2THz [8]–[10], with photon-triplets produced via processes involving SPDC having similar bandwidths.

However, it is to be noted that the photon triplets produced via Third Order SPDC or cascaded SPDC are extremely inefficient in experiments involving light-atom interactions. Due to photons produced via SPDC having broad bandwidth on the order of THz, using this technique to produce photons for interaction with atomic systems is difficult due to the optical transitions of such systems having lifetime limited bandwidth on the order of MHz. For light-atom interactions the photons produced must have bandwidth that matches atomic linewidths on the order of MHz, as if an individual photon's frequency does not fall within this atomic linewidth range, it cannot interact with the atom. The bandwidth of SPDC produced photons can be reduced by various filtering techniques such as optical cavities [11], [12], but this comes with trade-offs such as decrease in photon counts or brightness. With this problem in hand, the objective is to work towards a narrow-band photon triplet source that matches atomic linewidths.

Hence with this project, we work towards a proposed scheme for six-wave mixing (SWM) using Rubidium-87 to generate narrow-bandwidth photon triplets. This SWM scheme will be using light-atom interactions to produce photon triplets, and as such photons being produced will have

bandwidths matching the linewidths of Rubidium-87 transitions[13] on the order of MHz.

For the duration of this FYP, the goal is to determine if it is possible to filter and extract photon triplets out for detection through this SWM scheme. If successful, further work can be done on this project towards building a photon triplet source via SWM.

II. Six-wave mixing

Six-Wave mixing, SWM is a parametric process, and forms a cycle leading back to the initial ground state it was prepared in.

An ^{87}Rb cloud is first trapped in a MOT initially at the $5S_{1/2}$, $F=2$ state, following which a 795nm pump beam is used to excite it to the $5P_{1/2}$, $F=1$ state, where it will decay to the $5S_{1/2}$, $F=1$ state, releasing a 795nm photon. Following which, two pump beams at 780nm and 776nm are used to excite the cloud to the $5P_{3/2}$, $F=2$ and $5D_{3/2}$, $F=3$ states respectively. Here the atoms can decay back to its initial ground state, releasing a 762nm and a 795nm photon.

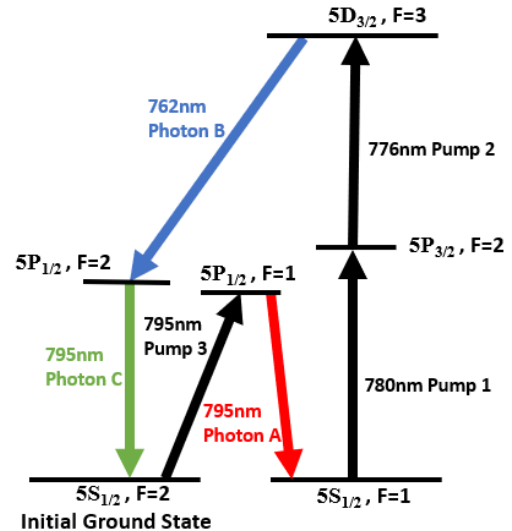


Figure 1: Energy Level Diagram of Six-Wave Mixing Scheme. The black arrows represent Lasers with frequencies matching the atomic transition, while the blue, green and red arrows represent photons generated from this scheme. The system is initially prepared in $5S_{1/2}$, $F=2$ ground state.

The SWM process is a parametric process, where energy and momentum are conserved. The energy conservation equation for the SWM process can simply be given as follows.

$$\hbar\omega_1 + \hbar\omega_2 + \hbar\omega_3 = \hbar\omega_A + \hbar\omega_B + \hbar\omega_C \quad 1$$

Here $\hbar\omega_i$ is the energy of the photons involved in the SWM process for an atom, with indices 1, 2, 3 referring to pump photons, and indices A, B, C referring to generated photons. This is in accordance with the energy levels of ^{87}Rb , and essentially is the premise of the SWM process. In the case of momentum conservation, the sum of the wave vectors \vec{k} of the photons is given as follows, with the indices 1,2 and 3 referring to pump photons and A, B and C referring to generated photons as before.

$$\vec{k}_1 + \vec{k}_2 + \vec{k}_3 = \vec{k}_A + \vec{k}_B + \vec{k}_C \quad 2$$

This equation combined with the energy conservation equation allows one to determine what direction the emitted photons will be in. The photons that are detected in certain directions will in theory exhibit strong time correlation, and uncorrelated fluorescence if detected any other direction. This direction that the time-correlated photons are emitted in can be found by phase matching conditions that arise from solving this momentum conservation equation.

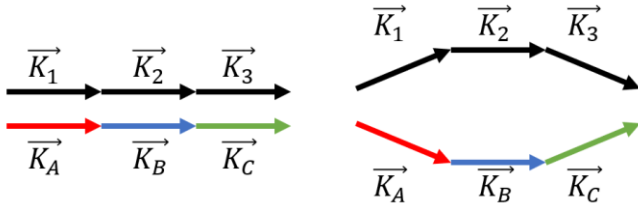


Figure 2: Two possible phase matching solutions for pump photons (1, 2, 3) and generated photons (A, B, C). (Left) Pump and generated photon momentums in collinear geometry. (Right) Phase matching for angle between pump and generated photon momentums.

There are numerous possible ways to orient the pump lasers and the direction of the generated photons. One such arrangement is a collinear arrangement, a trivial solution where all of the photon's momentum are oriented in the same direction, allowing for the lasers and generated photons to be coupled into a single mode fibre. The atomic transition lasers and generated photons will then need to be separated via the use of filtering techniques for the generation of a photon triplets, due to all of them having the same direction of propagation.

III. Filtering Photons Produced in Six-Wave Mixing

From the Six-Wave mixing experiment, it can be seen that there are 6 photons involved in this process. Three of which are from a narrowband laser source matching ^{87}Rb transitions, and the remaining three being generated photons produced from the wave mixing process. A collinear geometry will be used for this process, and so this would mean that the generated photons will need to be separated from the photons produced by a laser source in order to have a functioning photon triplet source. The wavelengths of these photons involved are as follows, rounded to the nearest nm.

	Transition	Photon Wavelength
Photons from Laser Source	$5S_{1/2}, F=1 \rightarrow 5P_{3/2}, F=2$	780nm
	$5P_{3/2}, F=2 \rightarrow 5D_{3/2}, F=3$	776nm
Generated Photons	$5D_{3/2}, F=3 \rightarrow 5P_{1/2}, F=2$	762nm
	$5P_{1/2}, F=2 \rightarrow 5S_{1/2}, F=2$	795nm
Photons from Laser Source	$5S_{1/2}, F=2 \rightarrow 5P_{1/2}, F=1$	795nm
Generated Photons	$5P_{1/2}, F=1 \rightarrow 5S_{1/2}, F=1$	795nm

Here the objective is to separate the generated photons from the laser source. In order to do this, some filtering methods need to be explored. It is found that commercially available interference filters are able to separate photons 2-3 nm apart from each other, and that means that the 780nm, 776nm and 776 photons can be separated from the bunch without much complexity. The problem that arises now is the question of separating the 795nm wavelength. These 795nm wavelengths are as follows.

Photon from Laser	794.98533 nm
Generated Photon	794.98361 nm
Generated Photon	794.97093 nm

And so, the focus now is to determine if it is possible to separate these wavelengths at 795nm. To find an optimal solution, a quantitative study is first done on existing filtering techniques used to separate differing wavelengths. An additional constraint to take note of is that the generated photons are estimated to have an intensity 12 orders smaller than the laser source, with a count rate of about 500 photons per second. This would mean that the filtering technique of choice need to be capable of separating wavelengths less than 2 picometers apart, suppressing the laser's intensity by 12 orders if required, as well as ensure maximum transmission of generated photons due to its low count rate. One such method of filtering photons that could match these criteria is the use of a Fabry-Perot Cavity, which was investigated through this project.

IV. Fabry Perot Cavity

A Fabry Perot cavity consist of two reflective surfaces, with the cavity simply being the region between these two surfaces. Sending light into such a cavity allows for light interference to occur within the cavity. Certain wavelengths are resonant to the cavity based on the cavity's length, and these resonant wavelengths will be transmitted through the cavity, with other non-resonant frequencies being attenuated. This would mean that the objective of such a cavity will be to constructively interfere for the wavelengths of generated photons, and destructively interfere and attenuate the wavelengths of the laser source.

The frequencies that are resonant within the cavity have a property of being equally spaced apart and is also known as the Free-Spectral Range Making the conversion from wavelength to frequency one finds that the 2pm difference in wavelength corresponds to a $\sim 0.8\text{GHz}$ difference in frequency. A property of the Free-Spectral Range is that the midpoint of this range generally corresponds to a point of maximum attenuation. And hence we find that in order to satisfy this criterion of maximum attenuation for the laser

source, the Free-Spectral Range of such a cavity should be $\sim 1.6\text{GHz}$. The relationship between length of a cavity and the Free-Spectral Range is given as follows.

$$\nu_{FSR} = \frac{c}{2L} \quad 3$$

Here ν_{FSR} is the Free-Spectral Range, L is length of the cavity and c is the speed of light. From this equation, one finds that the length of such a cavity is about 0.1m , which is a reasonable scale, and so the use of cavities in separating wavelengths 2pm apart can be investigated.

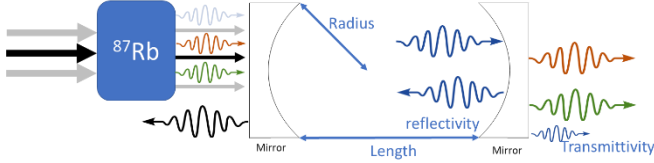


Figure 3: Fabry Perot Cavity separating generated photons and pump photons. Wavelengths resonant with cavity are transmitted and non-resonant wavelengths are reflected away. Factors of a cavity that affect the transmittivity of a wavelength are length of cavity, radius of mirrors, and reflectivity/ transmittivity coefficients of mirrors

A Fabry-Perot cavity can be characterized by the following properties, the length of the cavity or the distance between the mirrors, the radius of curvature of the mirrors, and the reflectivity and transmittivity of the mirrors. These physical properties of the cavity determine the transmittivity of wavelengths, and also the gaussian mode of a beam that can be transmitted through the cavity.

The transmission intensity of a resonator is given by following equation, which can be derived from the Airy formula [14]([Vol. 179, Chap. 1, pp. 1 – 60.) In this equation, t_1, t_2 and r_1, r_2 are the two mirrors transmission and reflection coefficients, I_0 is the intensity of the incident beam on the cavity, and $\Delta\nu$ is the difference between the closest allowed frequency $\nu_{q00} = \frac{c}{2L} \left[q + \frac{1}{2} \right]$ and the frequency of the incident beam.

$$I_t(\Delta\nu) = \frac{t_1 t_2}{(1 - \sqrt{r_1 r_2})} \frac{I_0}{1 + \frac{4\sqrt{r_1 r_2}}{(1 - \sqrt{r_1 r_2})^2} \sin^2 \left(\frac{\pi \Delta\nu}{\nu_{FSR}} \right)}$$

This allows for the graphing of the transmission vs frequency profile of the output light beam as shown in figure 8. It is to be noted that the transmission is simply given by $I_t(\Delta\nu)/I_0$. With reference to figure 8, the frequency difference between transmission peaks is the FSR frequency, and with a lower reflectivity coefficient, the full width half maximum (FWHM) frequency range increases. Since the objective of the Fabry Perot cavity is to allow transmission of one frequency and ensure minimal transmission for another, one may try to optimize parameters such as cavity length and reflectivity in order to ensure that the frequency for transmission is at a peak and is an allowed frequency, while the frequency to be blocked is at a transmission minimum in the cavity.

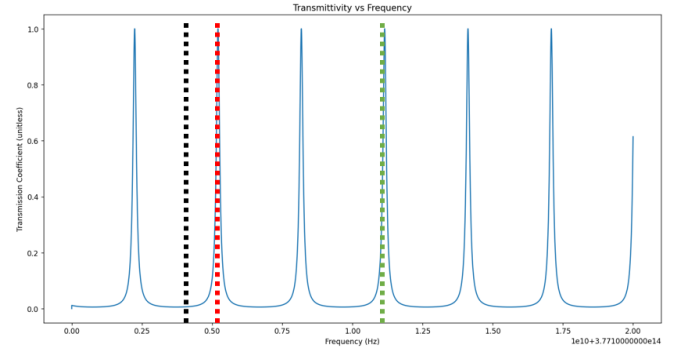


Figure 4: Simulation of Fabry-Perot cavity transmission profile with respect to six wave mixing experiment. Vertical dashed lines represent the three frequencies in six-wave mixing scheme at 795nm to be separated via a cavity; black represents pump beam, orange and green represent generated photons. Pump beam is to be attenuated and separated, hence close to a minimum on plot, generated photons to be transmitted via cavity, hence at a maximum on plot

The cavity should be able to transmit photons with a bandwidth of 20MHz (cavity FWHM should match photon bandwidth) and have a FSR of 1.6GHz . This lead to the physical parameters of the cavity length being $\sim 9.2\text{cm}$ and mirrors chosen for this cavity having a reflectivity of 97% .

To match the gaussian mode of an incoming beam into the cavity with the allowed gaussian mode within the cavity, focusing lenses need to be used to transform a gaussian beam output from a single mode fibre into the correct cavity mode. As such, the placement of the focusing lens as well as its focus lens will have to be determined. Simulations were performed to obtain the distance and focal length of the lens, as shown in Figure 5.

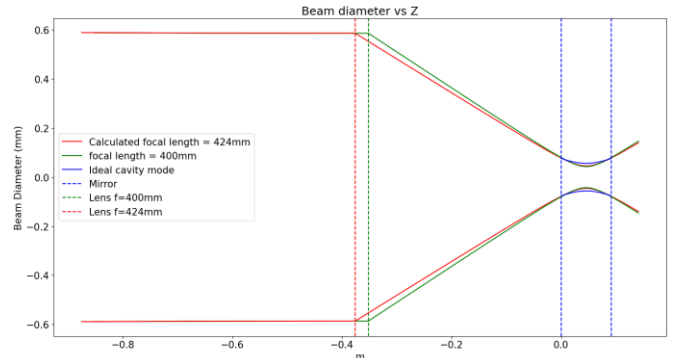


Figure 5: Plot showing the beam diameter of a collimated beam passing through a lens and matching the mode inside a cavity. Red and green dotted vertical lines represent position of 424mm and 400mm focal length lenses, and blue dotted vertical lines represent the position of mirrors of the cavity. Blue solid lines indicate the ideal cavity mode of a stable cavity.

V. External Cavity Diode Laser (ECDL)

Before building a Fabry-Perot Cavity, it is first necessary to obtain a photon source that is able to match the photons produced in the six-wave mixing scheme. This will be required for measurements on transmittivity and attenuation within a Fabry-Perot cavity. This photon source needs to be frequency stabilised as well as narrowband on the order of MHz . This criterion can be met by the use of External Cavity Diode Lasers.

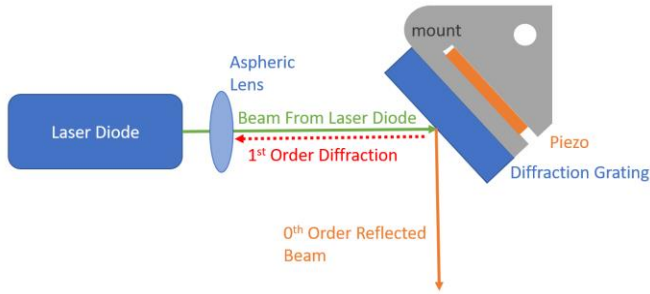


Figure 6: Schematic of an External Cavity Diode Laser (ECDL) in Littrow configuration [15]. An external cavity is formed between diffraction grating and laser diode by having first order diffracted beam reflect to the laser diode. Amplification of 1st order beam frequency in laser diode’s gain medium allows for $m=1$ diffracted wavelength to be the dominant wavelength in zeroth order reflection out of the ECDL. Mount is secured onto a surface, piezo is used to change angle of diffraction grating with respect to incoming beam by making small deflections in mount structure.

The External Cavity Diode Laser has a linewidth as well as frequency tuneable to the order of MHz. The objective now is to test a Fabry-Perot Cavity’s suitability for Six-Wave mixing using this laser. As such this laser should have frequency matching the frequency of a generated photon in this scheme. One way is to use a PID controlled frequency stabilisation using the Pound-Drever Hall technique. In this technique, the laser is frequency modulated with an Electro-Optical modulator to have additional side bands, and the beam is passed through an ⁸⁷Rb vapor cell, and then collected by a transimpedance amplifier. If the frequency of the laser is close to the transition frequency of the ⁸⁷Rb, a portion of the beam will be absorbed and scattered by the ⁸⁷Rb atoms in the vapor cell.

The beam intensity is converted to a voltage signal, which is then mixed with a phase shifted local oscillator signal. This provides an error signal that indicates how far off from a ⁸⁷Rb transition the beam’s frequency is. With this error signal, a PID response can be sent to the piezo inside the External Cavity Diode Laser to adjust the frequency to that of the ⁸⁷Rb transition. ⁸⁷Rb Spectroscopy in the 795nm regime was also performed via this error signal obtained by scanning a range of frequencies, as shown in Figure 7.

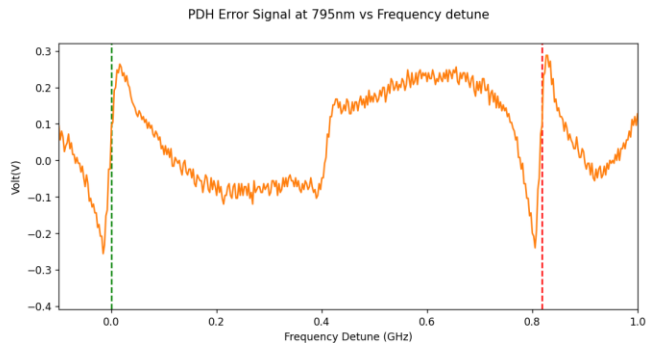


Figure 7: Plot of error signal at 795nm transition for ⁸⁷Rb, green dotted line (left) indicates the frequency at which $5S_{1/2}, F=2 \rightarrow 5P_{1/2}$, $F=2$ transition occurs, and the red dotted line indicates the $5S_{1/2}, F=2 \rightarrow 5P_{1/2}, F=1$ transition. The energy of these transmissions match that of a signal photon and pump photon respectively in the SWM experiment

VI. Fabry-Perot Cavity Set-up and Measurements

A Fabry-Perot Cavity was built based on the specification described in Section IV, with the cavity being

temperature stabilized and the length of cavity being adjusted by a piezo with a sub-micron step size. This piezo was attached to one of the mirrors within the cavity, with the other mirror being fixed to a spot.

The light output from the External Cavity Diode Laser locked to an ⁸⁷Rb transition was coupled into a single mode fibre and transmitted to the cavity, ensuring the beam had a gaussian profile. Cavity alignment was first done by using a CMOS camera to roughly get a gaussian profile within the cavity, and then via a photodetector attached to an oscilloscope. The laser was used to scan the 795nm frequency range and plot the transmission profile of the cavity, as shown in Figure 8. Upon rough alignment of the cavity, the laser was set back to the transition frequency of ⁸⁷Rb and using the Pound-Drever Hall technique and PID response to the cavity piezo, the length of the cavity was stabilised to be resonant with the frequency output from the laser.

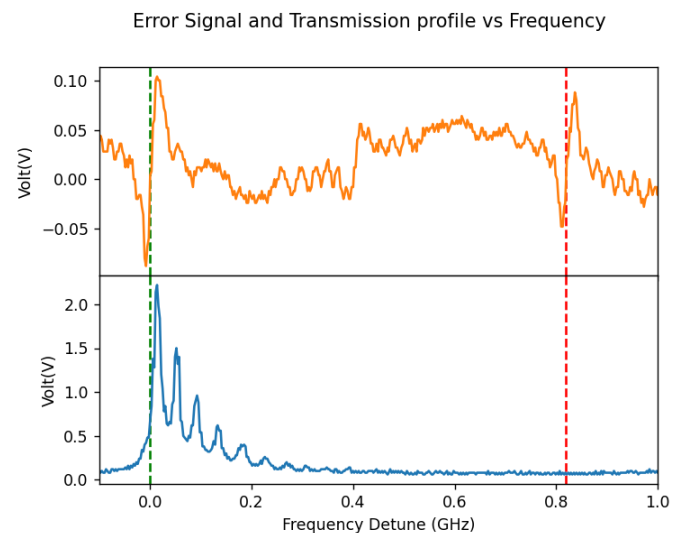


Figure 8: Error Signal and Transmission profile through a detuned Cavity vs frequency overlaid together. X-axis is frequency detune from the frequency that the cavity needs to transmit. The top plot shows ⁸⁷Rb spectroscopy in the 795nm regime. Refer to Figure 13 for details on top plot. Bottom plot shows transmittivity vs frequency detune, with vertical green and red lines showing regions where the transmission profile should be a maximum and minimum respectively.

A powermeter was used to measure the transmission coefficient by measuring the intensity of the beams before and after the cavity. This measurement gave a transmission coefficient of 0.3, which is far from the desired transmission coefficient of 0.9. One can see why this is the case by referring to Figure 20, where there can be multiple smaller peaks seen beside the highest peak (Frequency cavity is locked to). These peaks are formed due to higher order TEM modes, and this means that the total energy of the beam is being split across these TEM modes, hence resulting in a lower transmission coefficient. These higher order TEM modes have most likely appeared due to imperfect alignment of the cavity. It is to be noted that this cavity only had one degree of freedom (Length of cavity) in the form of a z-translation, and so by adding tip-tilt functionality to the mirrors of the cavity the higher order TEM modes could have been suppressed.

The second property that was of interest is the max transmission to attenuation ratio. In this case, transmission is measured at the frequency of a generated photon, while attenuation is measured at the frequency of the laser source.

This ratio was found to be 25. This number was expected to be approximately 2 orders as well, and as such, it is hypothesized that with a more robust cavity design this ratio can be maximised.

VII. Outlook

Simulation work done on Fabry-Perot cavities has shown that it is possible to use them for separation of the 795nm photons via narrow-band spectral filtering. An External Cavity Diode Laser (ECDL) has been built to emulate one of the generated photons to lock the cavity to. Following this a cavity was built to lock this ECDL, and its transmission coefficient for this ECDL as well as the transmission coefficients at a separate frequency (photon from laser source in Six-Wave Mixing meant to be separated) is measured.

The results obtained show that if this Fabry-Perot Cavity was to be used in the Six-Wave Mixing experiment, it would be able to attenuate the laser source's intensity by about 2 orders with respect to the generated photons intensity with a single cavity. However, the laser source's intensity is estimated to be about 12-13 times greater than that of the generated photons. As such it is estimated that about 5-6 such Fabry-Perot cavities will need to be chained together. However, the cavity design will need to be improved upon to ensure greater transmittivity and to eliminate the presence of higher order TEM modes within the cavity.

The Fabry-Perot Cavities will have to be locked using a narrowband laser at the same frequency as the generated photons. However, during the Six-Wave Mixing experiment, when a measurement is being made of the generated photons, the locking laser will have to be turned off, and during this measurement period when the laser is turned off, the cavity will need to be stable enough to not detune from the required resonant frequency. This stability can be ensured by adjusting the PID controls that control cavity length using a piezo. The objective of these PID adjustments would be to ensure that the cavity does not go out of lock due to a fast PID response.

Additionally, the measurement should only take place after a short delay from when the locking laser is turned off. This delay is to allow for the light trapped within the cavity to dissipate. To determine how long this time delay should be, one needs to refer to the cavity ring-down time, which is the time required to light intensity within the cavity to drop to $1/e$ of its initial intensity. Depending on the power of the locking laser, sufficient time must be given to allow the photon count from the locking laser to drop below the generated photon count (estimated to be 500 counts per second).

VIII. REFERENCES

- [1] J. Persson, T. Aichele, V. Zwiller, L. Samuelson, and O. Benson, "Three-photon cascade from single self-assembled InP quantum dots," *Phys. Rev. B*, vol. 69, no. 23, p. 233314, Jun. 2004, doi: 10.1103/PhysRevB.69.233314.
- [2] J. Douady and B. Boulanger, "Experimental demonstration of a pure third-order optical parametric downconversion process," *Opt. Lett.*, vol. 29, no. 23, p. 2794, Dec. 2004, doi: 10.1364/OL.29.002794.
- [3] T. E. Keller, M. H. Rubin, Y. Shih, and L.-A. Wu, "Theory of the three-photon entangled state," *Phys. Rev. A*, vol. 57, no. 3, pp. 2076–2079, Mar. 1998, doi: 10.1103/PhysRevA.57.2076.
- [4] M. Corona, K. Garay-Palmett, and A. B. U'Ren, "Third-order spontaneous parametric down-conversion in thin optical fibers as a photon-triplet source," *Phys. Rev. A*, vol. 84, no. 3, p. 033823, Sep. 2011, doi: 10.1103/PhysRevA.84.033823.
- [5] M. G. Moebius *et al.*, "Efficient photon triplet generation in integrated nanophotonic waveguides," *Opt. Express*, vol. 24, no. 9, p. 9932, May 2016, doi: 10.1364/OE.24.009932.
- [6] H. Hübel, D. R. Hamel, A. Fedrizzi, S. Ramelow, K. J. Resch, and T. Jennewein, "Direct generation of photon triplets using cascaded photon-pair sources," *Nature*, vol. 466, no. 7306, pp. 601–603, Jul. 2010, doi: 10.1038/nature09175.
- [7] D. C. Burnham and D. L. Weinberg, "Observation of Simultaneity in Parametric Production of Optical Photon Pairs," *Phys. Rev. Lett.*, vol. 25, no. 2, pp. 84–87, Jul. 1970, doi: 10.1103/PhysRevLett.25.84.
- [8] P. G. Kwiat, K. Mattle, H. Weinfurter, A. Zeilinger, A. V. Sergienko, and Y. Shih, "New High-Intensity Source of Polarization-Entangled Photon Pairs," *Phys. Rev. Lett.*, vol. 75, no. 24, pp. 4337–4341, Dec. 1995, doi: 10.1103/PhysRevLett.75.4337.
- [9] C. Kurtsiefer, M. Oberparleiter, and H. Weinfurter, "High-efficiency entangled photon pair collection in type-II parametric fluorescence," *Phys. Rev. A*, vol. 64, no. 2, p. 023802, Jul. 2001, doi: 10.1103/PhysRevA.64.023802.
- [10] T. Kim, M. Fiorentino, and F. N. C. Wong, "Phase-stable source of polarization-entangled photons using a polarization Sagnac interferometer," *Phys. Rev. A*, vol. 73, no. 1, p. 012316, Jan. 2006, doi: 10.1103/PhysRevA.73.012316.
- [11] A. Haase, N. Piro, J. Eschner, and M. W. Mitchell, "Tunable narrowband entangled photon pair source for resonant single-photon single-atom interaction," *Opt. Lett.*, vol. 34, no. 1, p. 55, Jan. 2009, doi: 10.1364/OL.34.000055.
- [12] A. Cerè, V. Parigi, M. Abad, F. Wolfgramm, A. Predojević, and M. W. Mitchell, "Narrowband tunable filter based on velocity-selective optical pumping in an atomic vapor," *Opt. Lett.*, vol. 34, no. 7, p. 1012, Apr. 2009, doi: 10.1364/OL.34.001012.
- [13] M. Steiner, V. Leong, M. A. Seidler, A. Cerè, and C. Kurtsiefer, "Photon bandwidth dependence of light-matter interaction," *Opt. Express*, vol. 25, no. 6, p. 6294, Mar. 2017, doi: 10.1364/OE.25.006294.
- [14] G. Gagliardi and H.-P. Loock, *Cavity-enhanced spectroscopy and sensing*. Heidelberg: Springer, 2014.
- [15] G. Lin, P.-Y. Su, and H.-C. Cheng, "Low threshold current and widely tunable external cavity lasers with chirped multilayer InAs/InGaAs/GaAs quantum-dot structure," *Opt. Express*, vol. 20, no. 4, p. 3941, Feb. 2012, doi: 10.1364/OE.20.003941.

Table of Contents

1	Motivation in generating Photon Triplets	4
1.1	Outline of Thesis	5
1.2	Previous Works in Four-Wave Mixing	6
1.3	Six-Wave Mixing	8
2	Filtering photons produced in Six-Wave Mixing.....	11
2.1	Feasibility of filtering using Interference Filters.....	12
2.2	Feasibility of filtering using Diffraction Gratings.....	12
2.3	Feasibility of filtering using Cavities	13
2.4	Components needed for testing using a Fabry-Perot Cavity	13
3	Frequency Stabilized Narrowband Lightsource: External Cavity Diode Laser	15
3.1	Laser Diode	16
3.2	Laser Driver	16
3.3	Threshold Current	17
3.4	Frequency Spectrum vs Current.....	19
3.5	Diffraction Grating Alignment.....	19
4	Frequency Stabilisation: Pound-Drever Hall Locking via Rubidium Spectroscopy.	22
4.1	Error Signal	24
5	Fabry Perot Cavity	29
6	Designing a Fabry-Perot Cavity.....	32
6.1	Length of Fabry-Perot Cavity	32
6.2	Reflectivity of Mirrors in Fabry-Perot Cavity.....	33
6.3	Radius of Mirrors in Fabry-Perot Cavity & Focusing Lens Parameters	33
7	Fabry-Perot Cavity Set-up	39
7.1	Cavity build.....	39
7.2	Cavity alignment setup.....	40
7.3	Cavity Alignment with Camera	40
7.4	Cavity Alignment with Oscilloscope and ⁸⁷ Rb Spectroscopy Signal.....	41
7.5	Pound-Drever Hall Locking of Cavity	43
7.6	Measurements and Results.....	44
8	Outlook: Incorporating Fabry-Perot Cavity into Six-Wave Mixing	46
9	Appendix 1: Optical components.....	47
9.1	Polarisers.....	47
9.2	Mirror	47
9.3	Beam Splitter (BS)	47
9.4	Wave Plate	48
9.5	Acousto-Optic Modulator (AOM)	48

9.6	Electro-Optic Modulator (EOM).....	48
10	Appendix 2: Non-Optical components.....	49
10.1	Powermeter	49
10.2	Optical Spectrometer.....	49
10.3	Function Generator.....	49
10.4	Oscilloscope	49
10.5	Wave Meter.....	49
10.6	Laser Driver	50
10.7	FM Board	50
11	Appendix 3: Six Wave Mixing Experimental Set-up.....	50
11.1	Pump Laser	51
11.2	Magneto-Optical Trap.....	51
11.3	Cooling Laser	52
11.4	Repump Laser	53
11.5	Calibration Lasers (762nm and 795nm).....	53
12	Appendix 4: Two-Photon Rubidium Spectroscopy	55
12.1	Preparing ^{87}Rb at $5P_{3/2}$, $F=2$ state.....	55
12.2	762nm External Cavity Diode Laser.....	55
12.3	Rubidium Spectroscopy using 762nm source	55
13	REFERENCES.....	59

Table of Figures

Figure 1: Four-Wave Mixing in ^{87}Rb cloud described by energy state diagram.....	7
Figure 2: Energy Level Diagram of Six-Wave Mixing in ^{87}Rb	8
Figure 3: Two possible phase matching solutions in Six-Wave Mixing.....	10
Figure 4: Schematic of an External Cavity Diode Laser in Littrow configuration	15
Figure 5: Histogram of temperature stability in External Cavity Diode Laser	16
Figure 6: Pictures of External Cavity Diode Laser	17
Figure 7: Threshold Current plots of Laser Diode	18
Figure 8: Optical Spectrum vs diode current plots.....	19
Figure 9: Image of ECDL housing showing grating and diode in Littrow configuration .	20
Figure 10: Pound-Drever Hall technique used to ECDL in Littrow configuration.....	22
Figure 11: Image of Pound-Drever Hall set-up mounted on optical table	24
Figure 12: Pound-Drever Hall Transfer function simulation	27
Figure 13: Plot of error signal vs frequency at 795nm transition for ^{87}Rb spectroscopy ..	28
Figure 14: Fabry Perot Cavity illustration.....	29
Figure 15: Simulation of Fabry-Perot cavity transmission profile.....	31
Figure 16: Simulation for mode matching between incident beam and cavity mode.	37
Figure 17: Picture of Fabry-Perot Cavity	39
Figure 18: Image of beam obtained from monochrome CMOS Camera placed at the end of a Fabry-Perot Cavity.....	41
Figure 19: Spectroscopy Signal and Transmission profile through a detuned Cavity vs frequency overlaid together	42
Figure 20: Spectroscopy Signal and Transmission profile through a tuned Cavity vs frequency overlaid together	43
Figure 21: Schematic of Set-up used to align and perform Pound-Drever Hall (PDH) Locking of the Fabry-Perot Cavity.	44
Figure 22: Four-Wave Mixing in ^{87}Rb cloud using collinear geometry.....	50
Figure 23: Set-up of Magneto-Optical Trap.....	52
Figure 24: Hyperfine energy level of ^{87}Rb D2 line with the target cooling and repump transitions.....	53
Figure 25 Pound-Drever Hall technique used with 2-photon spectroscopy to lock a 762nm External Cavity Diode Laser.....	56
Figure 26: Error Signal Trace obtained for 762nm regime via 2 photon spectroscopy in ^{87}Rb	57
Figure 27: Picture of iridescence observed from 2 photon spectroscopy in ^{87}Rb	58

1 Motivation in generating Photon Triplets

A photon triplet is a group of three photons produced from the same source. In the context of quantum optics, this means that they have the property of being time correlated. These photon triplet sources have become more popular over the years, finding uses in fields such as quantum cryptography, quantum computing as well as quantum teleportation[1]–[4]. In a similar fashion to photon triplets, there exists photon pair sources that produce two time-correlated photons from the same source. Many of the above-mentioned fields [5]–[9] such as quantum computing have been using photon pair sources due to robust pre-existing schemes of producing them such as Spontaneous-Parametric Down Conversion. However, in recent years with increased capabilities towards producing photon triplets there is more focus on the possible uses of photon triplets to replace photon pairs due to various advantages that using photon triplet sources can present.

There are several methods by which photon triplets can be generated[4]–[8], such as Third order SPDC, a process where a single photon is converted into three photons, or cascaded SPDC, a two-step cascaded photon-pair production process where a photon is split into a photon pair where one of the generated photons undergoes this process again to produce another photon pair forming a photon triplet[9].

In Spontaneous Parametric Down Conversion (SPDC), the production of photon pairs is described by the second order susceptibility $\chi^{(2)}$ of a non-linear crystal, a concept that shall be introduced in section 1.2. This process was first observed in [10] and has been the most widely used means of producing correlated photon pairs for the past few decades. This process allows for photon pairs to be produced in well-defined spatial modes, but with a broad bandwidth ranging from 0.1 to 2THz [11]–[13].

However, it is to be noted that the photon triplets produced via Third Order SPDC or cascaded SPDC are extremely inefficient in experiments involving light-atom interactions. Due to photons produced via SPDC having broad bandwidth on the order of THz, using this technique to produce photons for interaction with atomic systems is difficult due to the optical transitions of such systems having lifetime limited bandwidth on the order of MHz. For light-atom interactions the photons produced must have

bandwidth that matches atomic linewidths on the order of MHz, as if an individual photon's frequency does not fall within this atomic linewidth range, it cannot interact with the atom. The bandwidth of SPDC produced photons can be reduced by various filtering techniques such as optical cavities [14], [15], but this comes with trade-offs such as decrease in photon counts or brightness. With this problem in hand, the objective is to work towards a narrow-band photon triplet source that matches atomic linewidths.

Hence with this project, we work towards a proposed scheme for six-wave mixing (SWM) using Rubidium-87 to generate narrow-bandwidth photon triplets. This SWM scheme will be using light-atom interactions to produce photon triplets, and as such photons being produced will have bandwidths matching the linewidths of Rubidium-87 transitions[16].

Briefly describing this SWM scheme for producing photon triplets, a cold cloud of Rubidium vapor prepared by Doppler cooling with a Magneto-Optical Trap (MOT) is excited with three lasers with frequencies at various transitions of ^{87}Rb . The de-excitation of this cloud back to its initial ground state via a parametric process leads to three photons being emitted. Further descriptions of this SWM will be discussed in Chapter 1.3.

For the duration of this FYP, the goal is to determine if it is possible to filter photon triplets out for detection through this SWM scheme. If successful, further work can be done on this project towards building a photon triplet source via SWM.

1.1 Outline of Thesis

During the course of this FYP, work was done towards building External Cavity Diode Lasers (ECDL) frequency-stabilised for Rubidium-87 atomic transitions, along with Rubidium spectroscopy, as well as towards building a Fabry-Perot Cavity for narrowband filtering between photons with frequencies 0.8GHz apart. These works were done as part of working towards a triplet photon source via Six-Wave Mixing (SWM).

In Chapter 1, the motivations behind this project will be first explored. Following which the feasibility of such a project is shown via previous works done in Four Wave Mixing (FWM). The SWM scheme is then explained, where the properties of a photon triplet generated via this scheme is discussed.

In Chapter 2, the motivation behind narrowband filtering of photons is discussed, and various filtering techniques are explored, where we find the use of Fabry-Perot

Cavities to be the most practical filtering approach. A brief summary of what is needed to work towards building such a cavity is given, the main components needed being a frequency stabilized narrowband laser source and a cavity itself.

In Chapter 3, the process of building a narrowband laser source in the form of an External Cavity Diode Laser is described, with details on the working principals of this laser, characterisation of this laser as well as the building process.

In Chapter 4, the means via which frequency stabilisation of the narrowband laser is achieved is discussed. This frequency stabilisation is done via the Pound-Drever Hall method using Rubidium spectroscopy, of which more details is provided in this chapter.

In Chapter 5, the theory and working principals of a Fabry-Perot Cavity is discussed. Further investigation is also done via simulations and calculations on the feasibility of building such a cavity.

In Chapter 6, the design process of the Fabry-Perot Cavity is detailed, with calculations done to show how various parameter were set within the cavity, such as length of cavity, radius of curvature and reflectivity of mirrors within cavity.

In Chapter 7, the building and alignment process of the Fabry-Perot Cavity is discussed in greater details. The means via which measurements of transmission coefficients for the photons within this cavity were obtained is also detailed, with some discussions on the results that were obtained.

In Chapter 8, we conclude this report by discussing if the proposed method of using a Fabry-Perot Cavity will be a practical approach in the Six-Wave Mixing scheme for filtering between photons 0.8GHz apart.

1.2 Previous Works in Four-Wave Mixing

The Six-Wave Mixing (SWM) experiment will be built upon prior work done in Four-Wave Mixing (FWM) using ^{87}Rb , and since the experimental set-up for SWM simply has additional components that can be added by modifying a FWM experimental set-up, the FWM scheme is first discussed as a preliminary. FWM in non-linear fibres, hot vapor cells or cold atomic ensemble[17] allows for the generation of time-correlated photon pairs via nonlinear optical interactions in the material.

In nonlinear dielectric materials, the presence of an optical field polarises the material, resulting in a polarisation that can be written as follows[18].

$$P = \epsilon_0(\chi^{(1)}E + \chi^{(2)}E_2 + \chi^{(3)}E_3 + \dots) \quad 1.1$$

Here P is the polarisation in dipole moment per unit volume, E is the electric-field amplitude, $\chi^{(1)}$ is the linear first order susceptibility of the medium related to the refractive index of the material by $n = \sqrt{\chi^{(1)} + 1}$ and $\chi^{(n)}$ is the n-th order of non-linear susceptibility for the medium. In most cases the higher order terms are negligible, but not in the cases where field strength is high or in this case with the use of nonlinear material.

In comparison to SPDC, the discretisation of atomic energy levels results in photon pairs generated in FWM having a much narrower bandwidth compared to SPDC photons, being on the order of MHz[16], [19].

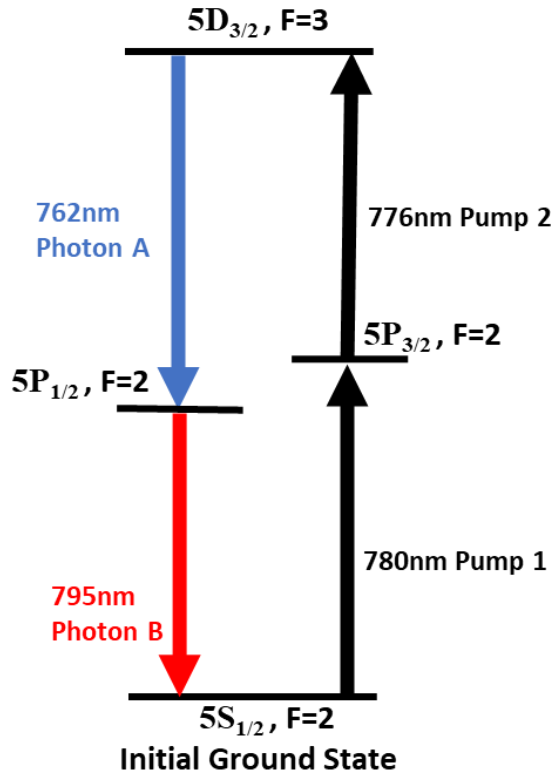


Figure 1: Four-Wave Mixing (FWM) in ^{87}Rb cloud described by energy state diagram. Arrows represent Photons. $5S_{1/2}, F=2$ ground state is excited to $5D_{3/2}, F=3$ by using 780nm and 776nm lasers. Cascade decay in ^{87}Rb back to initial ground state produces two photons, 762nm and 795nm.

In the FWM process, an ^{87}Rb atom is excited via two photons from laser sources, which results in the decay of this atom back to ground state emitting a photon pair. This FWM process is a parametric process, which means that the net effects of optical state transitions in the ^{87}Rb after this process leaves it unchanged in its initial ground state

without any transferring any additional energy or momentum. This concept is further explained in the next section, 1.3, with reference to the Six-Wave Mixing scheme.

1.3 Six-Wave Mixing

This section describes the proposed Six-Wave Mixing (SWM) scheme. As a preliminary, the energy levels of ^{87}Rb and energy momentum conservation of photons shall be briefly discussed to understand this scheme.

Similar to Four-Wave Mixing (FWM), SWM is a parametric process, and forms a cycle leading back to the initial ground state it was prepared in. The difference is that the SWM is a fifth order non-linear process, $\chi^{(5)}$, which would mean that the generated photon count through this process will be significantly lesser than that through the third order FWM process, estimated to be 6 orders lower, assuming excitation lasers with similar photon counts in both cases, the advantage being that this SWM process can generate time-correlated photon triplets.

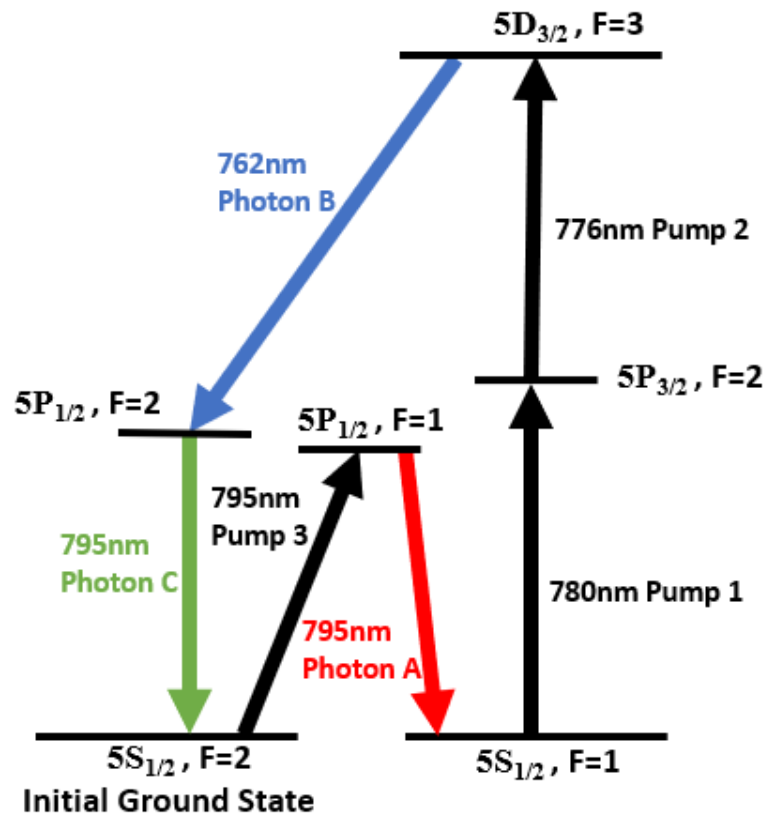


Figure 2: Energy Level Diagram of Six-Wave Mixing Scheme in ^{87}Rb . The black arrows represent photons from lasers, while the blue, green, and red arrows represent photons from deexcitation from this scheme. The system is initially prepared in $5S_{1/2}, F=2$ ground state.

An ^{87}Rb cloud initially at the $5S_{1/2}, F=2$ state, following which a 795nm laser is used to excite it to the $5P_{1/2}, F=1$ state, where it will decay to the $5S_{1/2}, F=1$ state, releasing a

795nm photon. Following which, two lasers at 780nm and 776nm are used to excite the cloud to the $5P_{3/2}$, $F=2$ and $5D_{3/2}$, $F=3$ states respectively. Here the atoms can decay back to its initial ground state, releasing a 762nm and a 795nm photon.

As described earlier, the SWM process is a parametric process, where energy and momentum are conserved. The energy conservation equation for the SWM process can simply be given as follows.

$$\hbar\omega_1 + \hbar\omega_2 + \hbar\omega_3 = \hbar\omega_A + \hbar\omega_B + \hbar\omega_C \quad 1.2$$

Here $\hbar\omega_i$ is the energy of the photons involved in the SWM process for an atom, with indices 1, 2, 3 referring to photons from laser sources, and indices A, B, C referring to generated photons. This is in accordance with the energy levels of ^{87}Rb , and essentially is the premise of the SWM process. In the case of momentum conservation, the sum of the wave vectors \vec{k} of the photons is given as follows, with the indices 1,2 and 3 referring to laser photons and A, B and C referring to generated photons as before.

$$\vec{k}_1 + \vec{k}_2 + \vec{k}_3 = \vec{k}_A + \vec{k}_B + \vec{k}_C \quad 1.3$$

This equation combined with the energy conservation equation allows one to determine what direction the emitted photons will be in. The photons that are detected in certain directions will in theory exhibit strong time correlation, and uncorrelated fluorescence if detected any other direction. This direction that the time-correlated photons are emitted in can be found by phase matching conditions that arise from solving this momentum conservation equation.

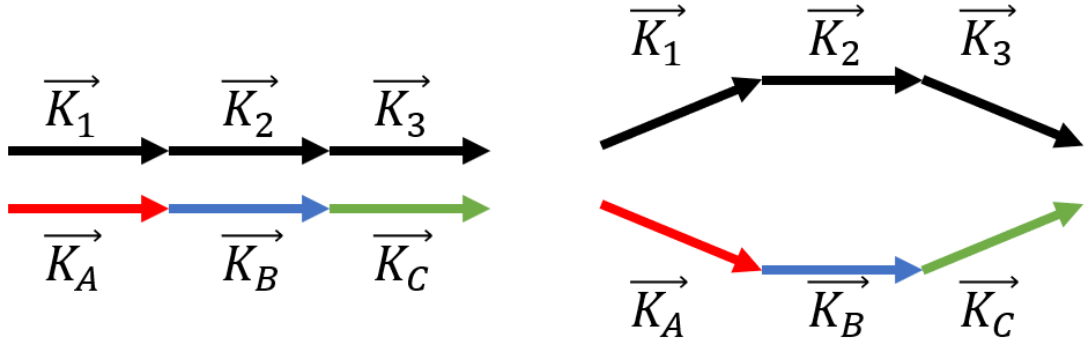


Figure 3: Two possible phase matching solutions for laser photons (1, 2, 3) and generated photons (A, B, C). (Left) Laser and generated photon momentums in collinear geometry. (Right) Phase matching for angle between laser and generated photon momentums.

It also shows that as long as momentum is preserved, there are numerous possible ways to orient the lasers and the direction of the generated photons. One such arrangement is a collinear arrangement, which allows for a trivial solution where all of the photon's momentum are oriented in the same direction, allowing for the lasers and generated photons to be coupled into single mode fibres in a convenient manner. Other configurations are possible however the photon momentums will be directed in a cone-like orientation, which makes collection of photons inefficient and difficult as only photons from a small section of this cone can be collected using a single fiber..

In the collinear arrangement, the laser's beam and generated photons will then need to be separated via the use of filtering techniques for the generation of a photon triplets. Filtering is now necessary to separate the laser and generated photons due to all of them having the same direction of propagation.

2 Filtering photons produced in Six-Wave Mixing

From the Six-Wave mixing experiment, it can be seen that there are 6 photons involved in this process. Three of which are from a narrowband laser source matching ^{87}Rb transitions, and the remaining three being generated photons produced from the wave mixing process. A collinear geometry will be used for this process, and so this would mean that the generated photons will need to be separated from the photons produced by a laser source in order to have a functioning photon triplet source. The wavelengths of these photons involved are as follows, with reference to Figure 2.

	Transition	Photon Wavelength (Rounded to nearest nm)
Photons from Laser Source	$5S_{1/2}, F=1 \rightarrow 5P_{3/2}, F=2$	780nm
	$5P_{3/2}, F=2 \rightarrow 5D_{3/2}, F=3$	776nm
Generated Photons	$5D_{3/2}, F=3 \rightarrow 5P_{1/2}, F=2$	762nm
	$5P_{1/2}, F=2 \rightarrow 5S_{1/2}, F=2$	795nm
Photons from Laser Source	$5S_{1/2}, F=2 \rightarrow 5P_{1/2}, F=1$	795nm
Generated Photons	$5P_{1/2}, F=1 \rightarrow 5S_{1/2}, F=1$	795nm

Here the objective is to separate the generated photons from the laser source. In order to do this, some filtering methods need to be explored. It is found that commercially available interference filters are able to separate photons 2-3 nm apart from each other, and that means that the 780nm, 776nm and 776 photons can be separated from the bunch without much complexity. The problem that arises now is the question of separating the 795nm wavelength. These 795nm wavelengths are as follows.

Photon from Laser	794.98533 nm
Generated Photon	794.98361 nm
Generated Photon	794.97093 nm

And so, the focus now is to determine if it is possible to separate these wavelengths. To find an optimal solution, a quantitative study is first done on existing filtering techniques used to separate differing wavelengths. An additional constraint to take note of is that the generated photons are estimated to have an intensity 12 orders smaller than

the laser source, with a count rate of about 500 photons per second. This would mean that the filtering technique of choice need to be capable of separating wavelengths less than 2 picometers apart, suppressing the laser's intensity by 12 orders if required, as well as ensure maximum transmission of generated photons due to its low count rate.

Some common filtering techniques that are generally used to separate light of different wavelengths include interference filters, diffraction grating and cavities.

2.1 Feasibility of filtering using Interference Filters

As mentioned commercially available interference filters are used for separating wavelengths 2-3nm apart or above. As such this would not be an ideal solution for separating wavelengths that are less than 2 picometers apart.

2.2 Feasibility of filtering using Diffraction Gratings

The next filtering technique one can look towards is via diffraction gratings. Diffraction gratings can separate an incoming beam of light by changing the angle at which the first order beams are reflected towards. The first drawback of this method is that the generated photons will not have a high detection efficiency due to losses from higher order diffractions and the zeroth order beam being unfiltered and hence unusable without further filtering. Assuming that this drawback can be mitigated, meaning that the first order diffraction still gives a significant enough photon count, one can check for the lines per mm required to separating the given wavelengths using a diffraction grating. The lines per mm of a reflective diffraction grating is the number of grooves present within one mm, meaning that the separation distance between grooves is simply given by 1mm / number of lines. Different wavelengths are refracted at differing angles formula given as follows, where d is the distance between grooves, θ_i is angle of incidence of the incoming light and θ_m is the angle for the m -th order diffraction.

$$d (\sin \theta_i - \sin \theta_m) = m\lambda \quad 2.1$$

Here $m = 1$, as we are interested in the first order diffraction. One finds that the parameter d needs to minimally be greater than λ , the wavelength. By a substitution of d as 800nm and $\theta_i = 0$ as normal incidence, one finds that the difference in separation angles for wavelengths 2pm apart is 10^{-7}° . This means that a rather unreasonable length on the order of 100s of kilometres will be required to obtain a separation of millimetres between the two wavelengths. This method of conventionally separating differing wavelengths is impractical and hence other methods need to be explored.

2.3 Feasibility of filtering using Cavities

Here, the practicality of using cavities to separate wavelengths picometers apart is investigated. The two types of cavities that can be discussed are Fabry-Perot cavities and solid etalons. Both of these cavities are essentially devices that consist of two reflective surfaces, with the cavity simply being the region between these two surfaces. Sending light into such a cavity allows for light interference to occur within the cavity. Certain wavelengths are resonant to the cavity based on the cavity's length, and these resonant wavelengths will be transmitted through the cavity, with other non-resonant frequencies being attenuated. This would mean that the objective of such a cavity will be to constructively interfere for the wavelengths of generated photons, and destructively interfere and attenuate the wavelengths of the laser source.

Considering the wavelengths that need to be attenuated or transmitted, some calculations can be performed to find that the length of such a cavity is about 0.1m, which is sized at a reasonable scale. The two mirrors' reflectivity in this cavity needing to be about 97%, which also is commercially available. This makes the use of Cavities the most and so the use of cavities in separating wavelengths 2pm apart can be investigated. Further details on how these numbers were obtained will be discussed in Chapter 6.

The main fundamental difference between solid etalons and Fabry-Perot Cavities is that the length of solid etalons is controlled by temperature whereas in Fabry-Perot Cavities it can be designed to be controlled by both temperature and by manually changing the length of the cavity using a piezo or other means. A solid etalon will need to also be manufactured to the length specification required which would be expensive as an investment for simply investigating the feasibility of such a filtering technique. Hence, due to the versatility of Fabry-Perot cavities in this regard, they have been chosen as the proposed method of filtering photons 2nm apart in wavelength.

2.4 Components needed for testing using a Fabry-Perot Cavity

It is to be noted that the main objective is to determine if a Fabry-Perot cavity is suitable for use in the Six-Wave Mixing experiment for detection of generated atoms. And as such, the objective now is to determine the transmission and attenuation coefficients that can be obtained from such a cavity, and then determine if it is possible to use such a cavity for Six-Wave Mixing.

Naturally, one would need to build such a cavity in order to test it. However, it is also important to find a light source that can replicate the properties of the generated photons. Such a light source will need to be at the frequency of the atomic transition of the generated photons/ laser to be used in Six-Wave Mixing. It will also be required to have a bandwidth on the order of MHz to replicate the bandwidth of photons generated via atomic transitions.

The proposed light source needs to be frequency stabilised as well as narrowband on the order of MHz. This criterion can be met by the use of External Cavity Diode Lasers, which was the light source that was used in this project. And so, in Chapters 3 and 4, the process of building such a light source is first discussed, and in Chapters 5 – 7, the process of building a Fabry-Perot Cavity is detailed.

3 Frequency Stabilized Narrowband Lightsource: External Cavity Diode Laser

The External Cavity Diode Laser (ECDL) is a set-up that consists of a single mode semiconductor laser diode, mounted in a housing with an aspheric lens and a diffraction grating in the Littrow configuration.

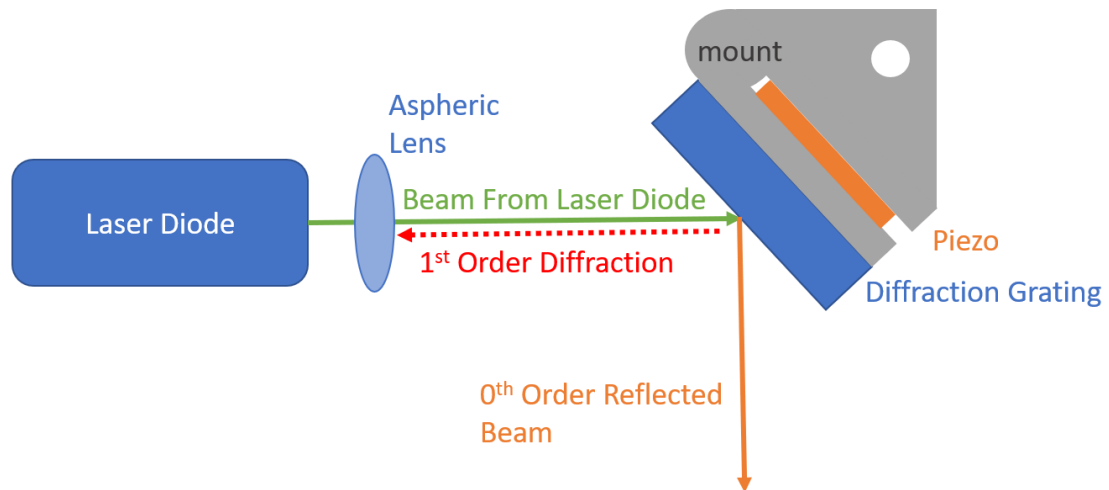


Figure 4: Schematic of an External Cavity Diode Laser (ECDL) in Littrow configuration [20]. An external cavity is formed between diffraction grating and laser diode by having first order diffracted beam reflect to the laser diode. Amplification of 1st order beam frequency in laser diode's gain medium allows for $m=1$ diffracted wavelength to be the dominant wavelength in zeroth order reflection out of the ECDL. Mount is secured onto a surface, piezo is used to change angle of diffraction grating with respect to incoming beam by making small deflections in mount structure.

In this configuration, the laser diode produces a beam that is collimated by the aspheric lens and travels to the diffraction grating. At the diffraction grating, the first order diffraction is directed back towards the laser diode, forming an external cavity between the diffraction grating and the laser diode. The laser diode itself produces a beam with a large bandwidth, and as such the purpose of the grating is to ensure that the ideal laser frequency can be directed back into the laser cavity as a first order diffraction beam. This allows for amplification of that selected frequency through the laser diode, which results in the output beam at the zeroth order diffraction from the grating being at the desired frequency.

The following subsections go into greater details on the building, characterisation, and the frequency-locking of an ECDL.

3.1 Laser Diode

First, a laser diode that would be able to produce a 795nm beam had to be selected. We use a LD808-SA100 laser diode with a spectrum that contained the said wavelength required as shown in Figure 10. Empirically, this laser diode has been used by the research group and found to be able to produce 795nm light at the ground state transitions of ^{87}Rb .

3.2 Laser Driver

A laser driver board was used to supply and regulate current to the laser diode. It is to be noted for future reference that when preparing the boards, one will need to consider the pin of the laser diode connected to the outside casing of the diode and verify if it is cathode or anode grounded. Based on the schematics of the laser diode found from the supplier catalogue[21], it was found that the LD808-SA100 laser diode was cathode grounded. Additional functionalities of this board included temperature control for the laser diode, which was achieved via having a thermistor read the temperature and a Peltier device attached to a heat sink. With the use of a PID feedback loop, the temperature can be stabilized to 5-8mK, as illustrated in the histogram in Figure 5.

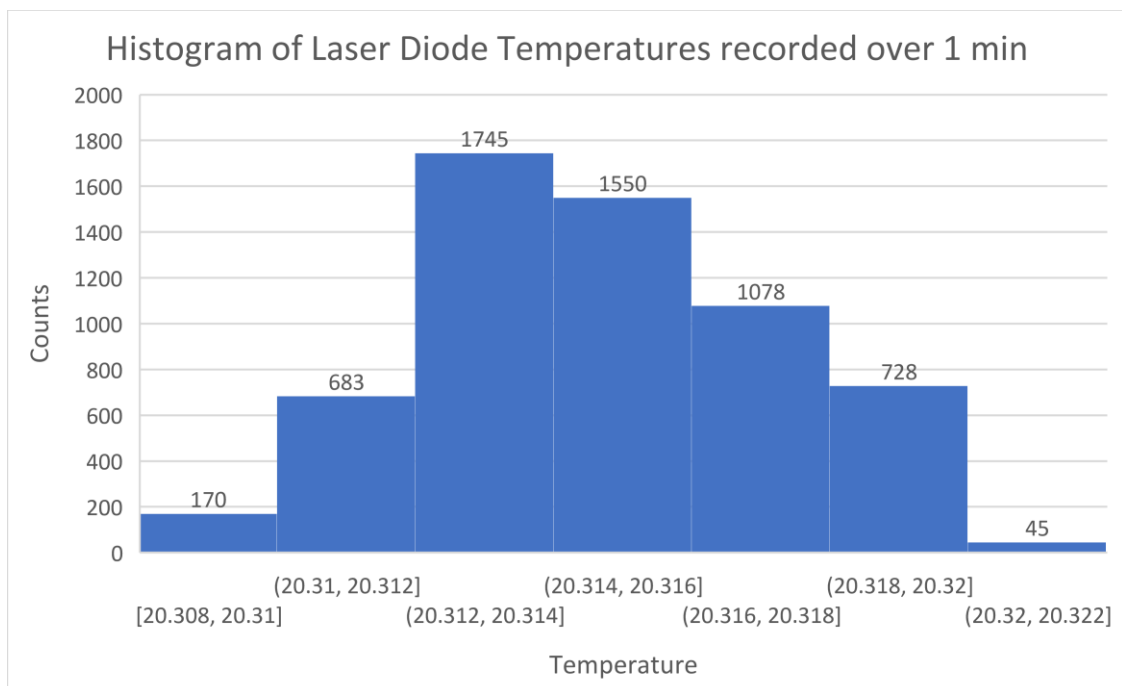


Figure 5: 6000 Datapoints for Laser Diode Temperatures were obtained over a period of 1 minute and fitted into a Histogram. The temperature of the Laser Diode was set to 20.315°C using a Peltier cooler and a thermistor to provide a PID cooling response to the Peltier. The Average and Mean temperatures were both found to be 20.315°C, with a standard deviation of 2.5mK.

A diffraction grating with 1800 lines per mm is placed in the beam path, with the $m=1$ diffracted beam being directed back into the laser diode to form the external laser cavity for amplification of the diffraction beam. The board also had a piezo attached to the diffraction grating mount that was used to control the diffraction gratings angle, which is necessary to achieve laser locking via the Pound-Drever Hall technique, which is explained later in Chapter 4. The laser driver board, the temperature control mechanism as well as the piezo with diffraction grating set-up was mounted within a housing unit.

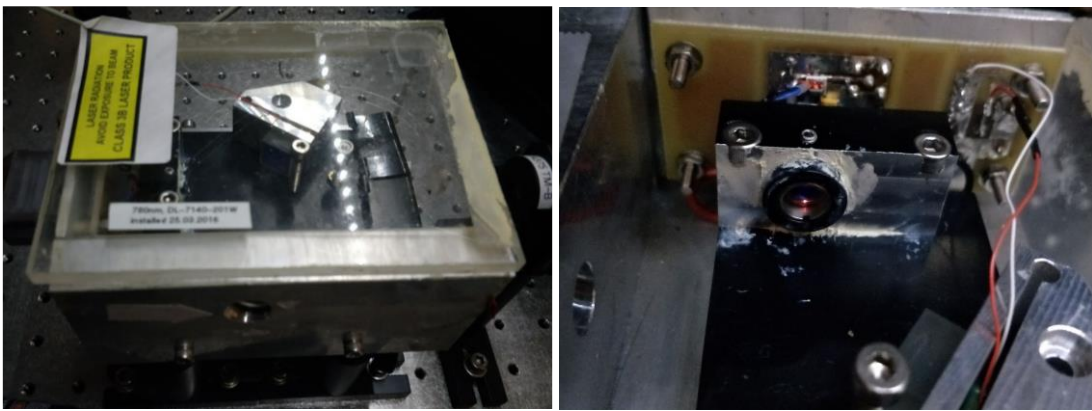


Figure 6: (Left) Picture of an ECDL with its housing (Right) Picture of inside of ECDL in Littrow configuration.

With the set-up, the laser diode was characterized via two main methods, first by finding the PI (power vs intensity) curve of the laser, and second by measuring the frequency spectrum of the laser at various diode currents. These methods enable us to find the Threshold Current, and the Frequency Spectrum vs Current.

3.3 Threshold Current

An important property for semiconductor laser diodes is its threshold current, which is defined as the current where the diode current at which lasing begins. This can be found from a plot of laser diode current vs light intensity, and in order to obtain such a plot, the following steps were taken.

A powermeter was used to measure the intensity of the laser light being produced by the laser diode, with the laser diode current being varied from 0mA to 140mA. Using

python to automate these measurements and plot the data, the following plot was obtained.

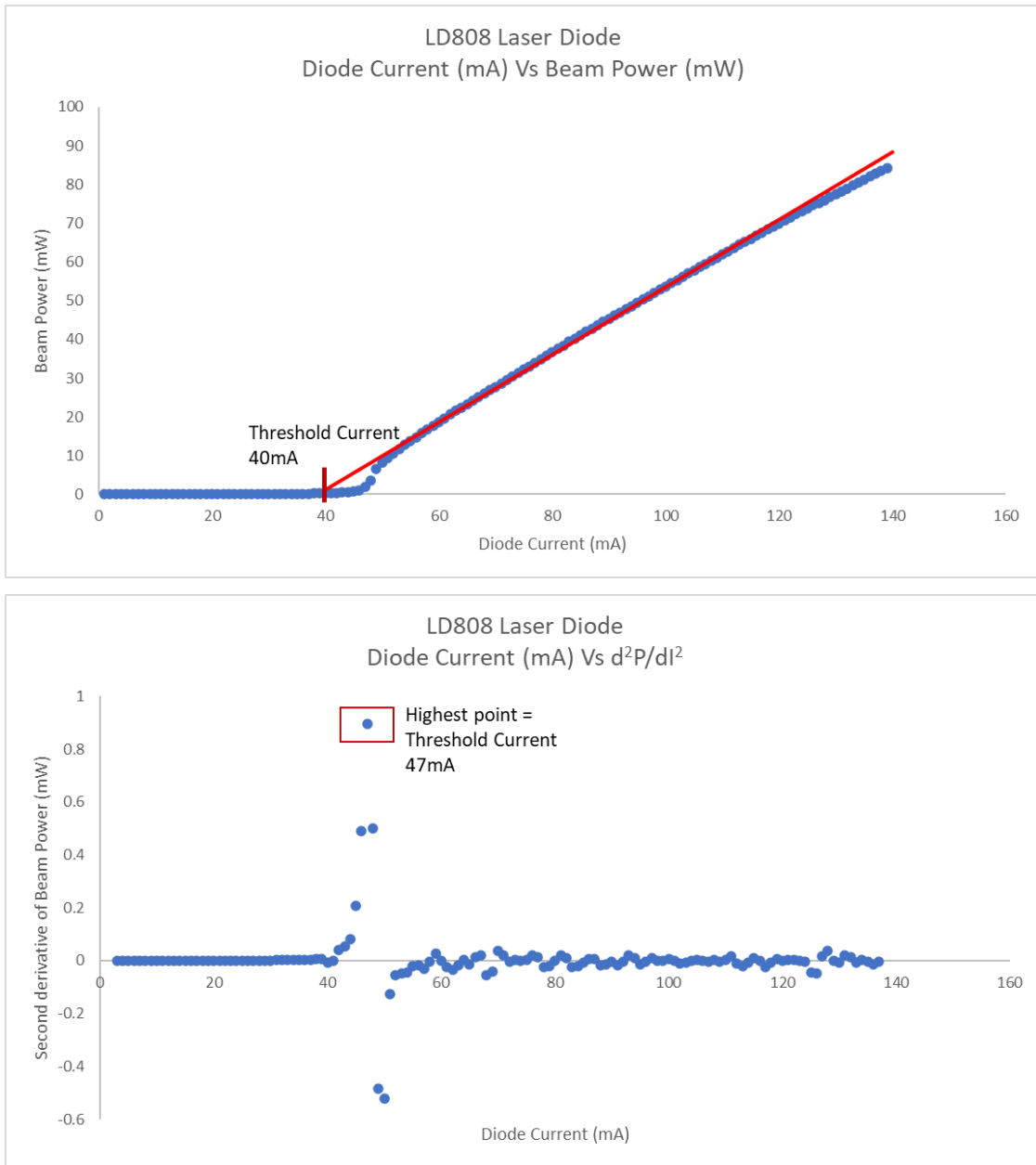


Figure 7: (Top) Plot of laser diode current (mA) vs power of beam (mW). Threshold current can be obtained for laser diode from these points. There are multiple accepted methods of finding Threshold current, such as linear extrapolation as shown in Figure. (Bottom) Plot of laser diode current (mA) vs second derivative of beam power (mW). Threshold is the highest point on this plot. This is the most commonly accepted method of finding Threshold current for laser diodes.

From the PI curve obtained, the threshold current of the laser diode can be obtained. This was found to be 40mA for the LD808 laser diode, as can be seen in Figure 7. There

are multiple accepted ways of finding the Threshold current[22] such as linear extrapolation as shown in 7(top), with the most common method being to plot the second derivative and find the highest point on the second derivative curve. d^2P/dI^2 . As seen from Figure 7 (bottom), the threshold current for the LD808 Laser diode was found to be 47mA.

3.4 Frequency Spectrum vs Current

Another important property of a semiconductor laser diode is its optical spectrum. It is important to determine if the laser has a spectrum that encompasses the desired frequency. To do so, an optical spectrometer was used to determine the spectrum for a given current. A useful observation that can be made is that changing the diode current also changes the spectrum and peak wavelength obtained from the spectrometer.

The frequency spectrum of the laser was obtained via using an Ocean Optics spectrometer to measure and plot the spectrum for various laser diode currents, as shown in Figure 8. This characterization allowed greater understanding on what diode currents should be used when trying to obtain the desired frequency.

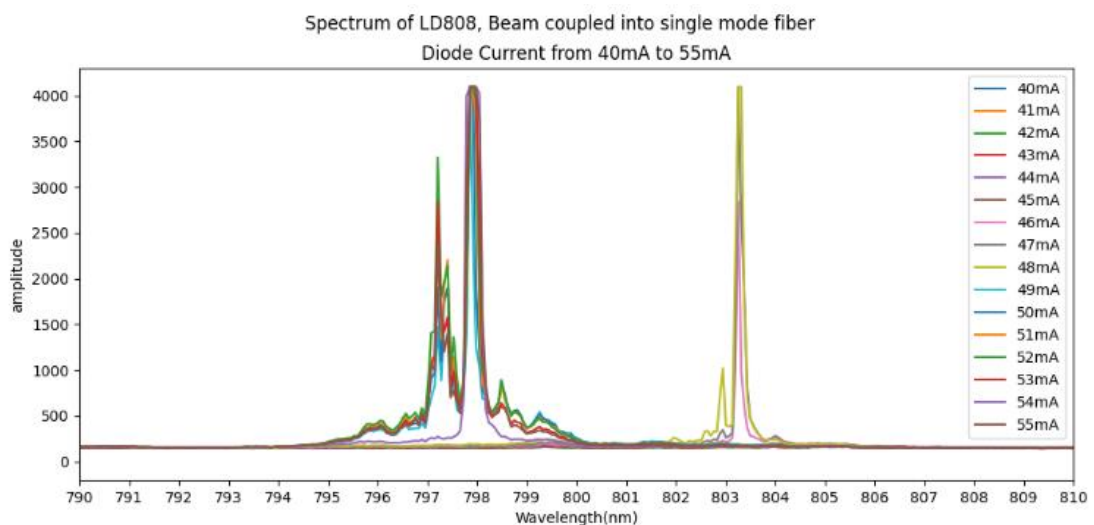


Figure 8: Spectrum of LD808 laser diode for Diode currents from 40mA to 55mA in increments of 1mA. Spectrum measured with Ocean Optics spectrometer with precision of 2nm. It can be seen that changing diode current can change the optical spectrum of beam; hence one can adjust diode current to select spectrum with desired peak wavelength.

3.5 Diffraction Grating Alignment

To selectively choose a frequency to output from the ECDL, a diffraction grating was used. As per the Littrow configuration, the diffraction grating diffracts the first order

beam back towards the laser diode. This results in the first order diffracted beam being sent back into the laser diode along the same beam path as the incident beam on the grating having a particular frequency. This frequency can be controlled by adjusting the angle at which the incident beam from the laser diode hits the grating.

The presence of this frequency within the laser's cavity allows for the amplification of that frequency within the diode's cavity, making it the dominant frequency that will be output from the laser diode. This results in the zeroth order beam being reflected from the grating having a peak frequency that is dependent on the angle at which the beam from the laser diode is incident on the diffraction grating.

A coarse adjustment must be made to ensure the first order diffracted beam from the grating is indeed going back into the laser diode. The precision to achieve here is on the order of degrees. Next a fine adjustment has to be made to select the frequency that is being output from the ECDL. An adjustment of approximately 0.06° change the frequency by 1nm. This precision in the angle can be derived from the diffraction equation for reflective gratings, which is as follows.

$$a(\sin \theta_n + \sin \theta_i) = n\lambda \quad 3.1$$

In the equation a refers to the groove separation distance of the grating, θ_n and θ_i are the angles made by the n th order diffraction and incident beams with respect to the normal of the grating. It is useful to note that the grating used had 1800 grooves per mm.

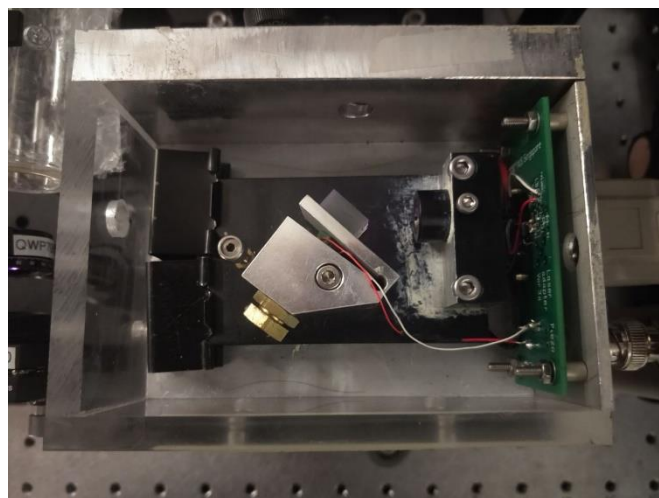


Figure 9: Image of ECDL housing showing grating and diode in Littrow configuration

To make the initial coarse adjustments to have the first order diffraction from the grating align with the incident beam from the laser diode, the following steps were undertaken. The first order beam was roughly aligned with the incident beam from the diode. Using a card with a hole roughly the same diameter as the beam size, align the hole with the incident beam from the laser diode. From there observe where the first order beam is being diffracted to onto the card. Adjust the grating as necessary to ensure that the first order beam passes through the same hole as the incident beam.

Next, with the use of a powermeter, the intensity of the zeroth order beam output from the ECDL is measured. In this step, the current being supplied to the diode is set to be slightly lower than the threshold current. As discussed earlier, the laser diode will produce a low intensity beam before reaching the threshold current. But due to the presence of an external cavity for the laser diode to build up its beam intensity via stimulated emission, the intensity of the output beam measured by the powermeter will drastically increase by an order when the first order beam is aligned with the incident beam.

To make fine adjustments to the grating, it is necessary to know the frequency that is being output from the ECDL. As such, the output beam from the ECDL is coupled into a wavemeter, where the peak wavelength from the ECDL is measured. An adjustment of approximately 0.06° change the frequency by 1nm, and so in order to make adjustment on this order, the grating was mounted on a custom mount that allowed for adjustments to the grating angle via a hex screw. This adjustment via the hex screw allowed for the frequency to be selected to an accuracy of 0.5nm. To reach an accuracy of 1pm, the temperature and diode current can be adjusted. It was found that a change of about 3K in temperature resulted in the peak wavelength shifting by approximately 1nm, which was found by varying the temperature and measuring the corresponding change in the peak wavelength.

4 Frequency Stabilisation: Pound-Drever Hall Locking via Rubidium Spectroscopy

In this section, the means via which the laser produced from the ECDL is locked to a particular frequency is explored. In this project, the frequencies of the lasers required for six-wave mixing are essentially transition frequencies of Rubidium. To simulate these transition frequencies, a laser needs to be locked to that frequency using a Rubidium cell and has to be stable at said frequency. In order to do so, the method by which the laser light is locked to the desired frequency via the Pound-Drever Hall technique through Rubidium spectroscopy. A schematic of how this is achieved is as shown below in Figure 10.

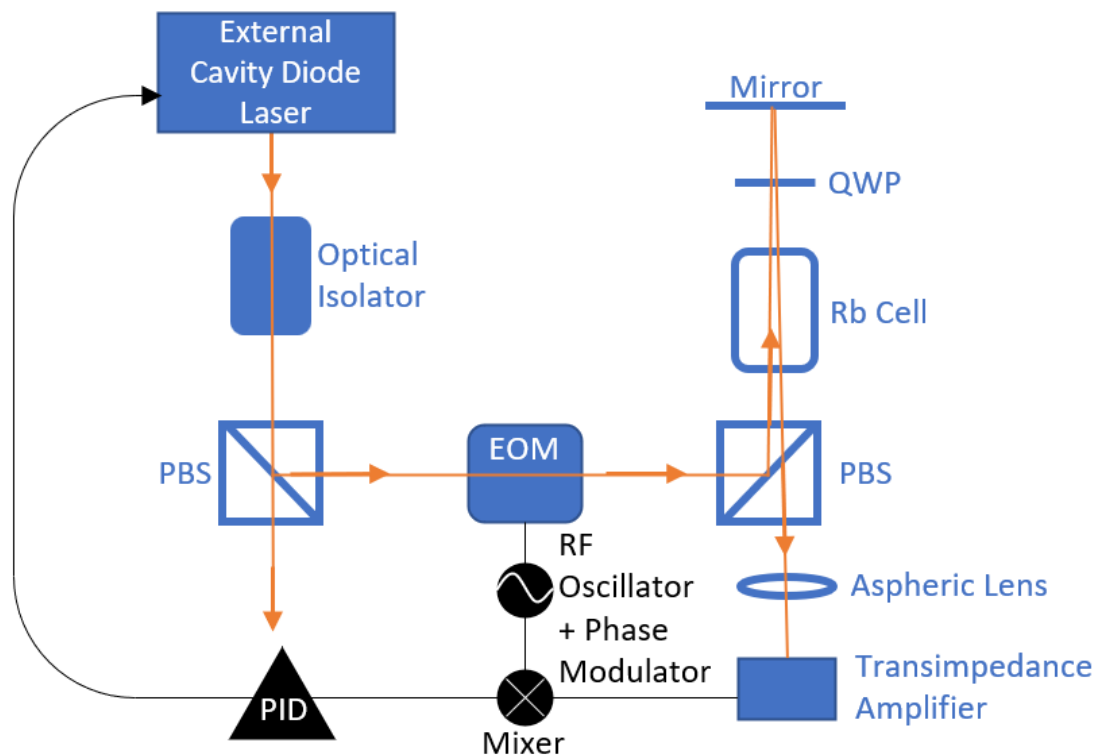


Figure 10: Illustration of Pound-Drever Hall set-up used to External Cavity Diode Laser (ECDL) in Littrow configuration. Orange beams with arrows indicate path taken by beam. Blue components represent optical components, black components represent electronic components/ response. EOM: Electro-Optical Modulator, PBS: Polarising Beam Splitter, QWP: Quarter Wave Plate, Rb Cell: ^{87}Rb vapor cell. Refer to Figure 4 for schematic of ECDL

To explain this method, one may try to follow the beam path from the laser. First the beam passes through an isolator to ensure that light beams do not get reflected back to the laser from the set-up. The beam is then split via a polarising beam splitter, with

one path to be used as an output beam, and the other to be used for the Pound-Drever Hall process. This beam passes through a phase modulator modulated by a local oscillator, in the case of this project an EOM (electro-optic modulator) modulated with a 22MHz sine wave from a function generator. The addition of this component results in the beam having two side band frequencies alongside its main carrier frequency from the laser.

The beam, now consisting of the phase shifted carrier frequency and two side bands, now travel through a quarter wave plate, and reach a Rubidium cell, where parts of the beam will be absorbed if it matches a ground state transition frequency. Following which the beam gets reflected off a mirror and travels through a quarter wave plate twice, changing the linear polarisation to allow for transmission through a beam splitter and into a photodetector, where the signal is mixed down with the local oscillator and phase shifted to give a PID feedback response indicating how far away from the ground state Rb transition frequency the carrier signal is. The PID signal would translate to a feedback signal to a piezo attached to the diffraction grating in the laser source box. What this diffraction grating would effectively do is change the angle at which the beam from the laser diode hits the grating, effectively changing the $m=1$ diffraction frequency and hence change the carrier frequency. This feedback loop hence allows the laser frequency to be stabilized and locked to a particular resonant frequency.

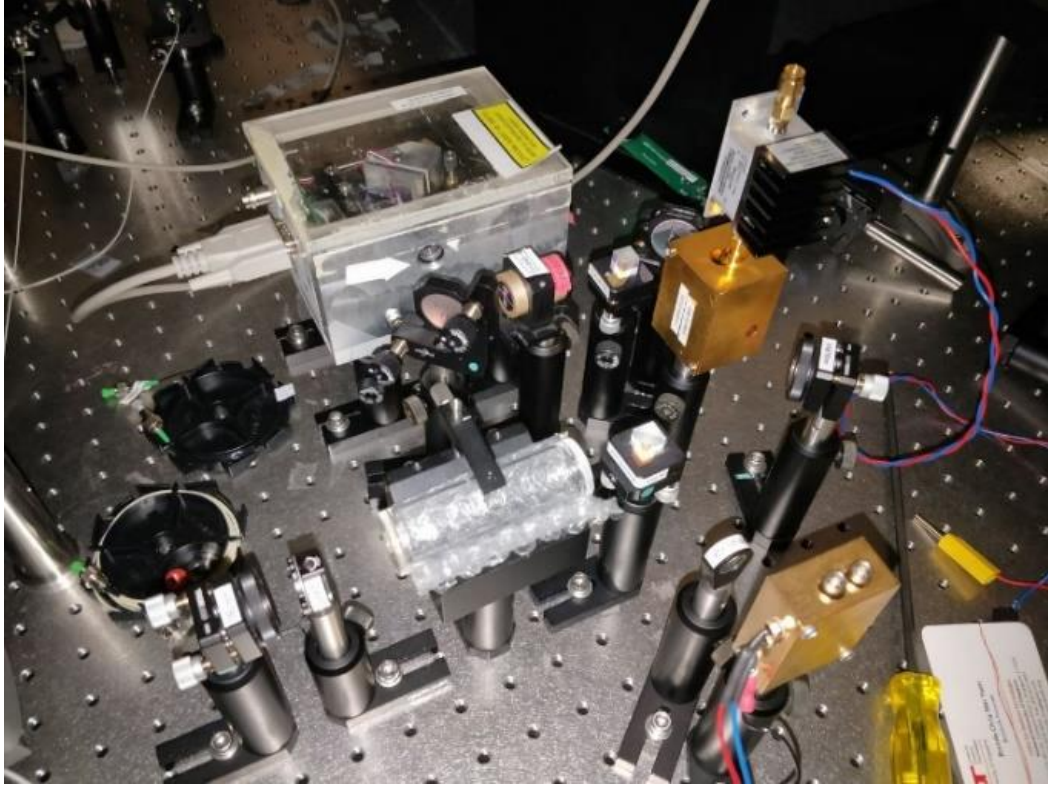


Figure 11: Image of External Cavity Diode Laser locked to an ^{87}Rb cell in a Pound-Drever Hall set-up mounted on optical table

Via this process, the LD808 diode was locked to an ^{87}Rb transition, namely the 795nm $F=2 \rightarrow 1$ transition found in the Six-Wave Mixing scheme. The lock is at present highly dependent on environmental factors, as external disturbances such as mechanical vibrations to the optical table of the set-up or fluctuations in temperature results in detuning from lock. The stability of the lock has been improved by fine tuning the PID values for the piezo as well as the Peltier cooler for temperature response.

4.1 Error Signal

This section details how an “Error Signal” that helps form the PID response for the piezo is made.

To form an error signal, the carrier signal is changed through a range of frequencies, and the output at the photodetector is measured. To explain this section in depth, one must look at the effects of pulse modulation by the EOM, and how the voltage output from the photodetector can be mixed with a phase delayed signal from the local oscillator to give an error signal.

Light beams can be described by their Electric fields as $E_0 e^{i\omega t}$, where E_0 is the amplitude of the field and $\omega = 2\pi f$ is the angular frequency of the field. After phase modulation by the EOM, this field takes on the following form.

$$E = E_0 e^{i(\omega t + \beta \sin(\omega_m t))} \quad 4.1$$

Here ω_m is the modulation frequency by the EOM. This additional phase essentially adds two sidebands with amplitude provided β is small enough, as can be seen after first order Taylor expansion. These resulting sidebands will be separated from the carrier frequency by $\pm\omega_m$.

$$\begin{aligned} E &= E_0 e^{i(\omega t + \beta \sin(\omega_m t))} \\ &= E_0 e^{i\omega t} [1 + i\beta \sin(\omega_m t)] \\ &= E_0 e^{i\omega t} \left[1 + \frac{\beta}{2} e^{i\omega_m t} - \frac{\beta}{2} e^{-i\omega_m t} \right] \end{aligned} \quad 4.2$$

Next, one can consider the transfer function for the beam passing through the Rubidium cell before heading into the photodetector. This transfer function R would simply be $R(\omega) = E_0/E_R(\omega)$, where $E_R(\omega)$ is the amplitude of the reflected beam passed through the Rubidium cell heading towards the photodetector. Keeping in mind this transfer function, it is useful to work out the optical power incident on the photodiode for this next part, which is given by $P \propto E_R E_R^*$.

$$\begin{aligned} P_R &= P_0 \left[|R(\omega)|^2 + \frac{\beta^2}{4} |R(\omega + \omega_m)|^2 + \frac{\beta^2}{4} |R(\omega - \omega_m)|^2 \right] \\ &\quad + P_0 \beta \{ \text{Re}[\chi(\omega)] \cos \omega_m t + \text{Im}[\chi(\omega)] \sin \omega_m t \} \\ &\quad + (2\omega_m \text{ terms}) \end{aligned} \quad 4.3$$

Here, $\chi(\omega) = R(\omega)R^*(\omega + \omega_m) - R^*(\omega)R(\omega - \omega_m)$. This is the quantity of interest, which is a measure of how close the carrier frequency is to the transition frequency. It is to note that the output signal from the photodetector V_R is proportional to P_R . V_R is mixed with a off phase signal from the local oscillator, $V'_R = V_R \cos(\omega_m t + \varphi)$, and passed through a low pass filter, removing any oscillating terms, and leaving behind a signal as follows.

$$V(\omega) \propto \text{Re}[\chi(\omega)] \cos \varphi + \text{Im}[\chi(\omega)] \sin \varphi \quad 4.4$$

By adjusting the phase φ it is possible to remove either the real or imaginary components, and via two modulation paths with $\varphi^1 = \varphi^2 + \frac{\pi}{2}$, it is possible to obtain $\chi(\omega)$.

The beforementioned error signal that allows one to form a PID feedback loop is indeed just a plot of frequency vs $\chi(\omega)$. To understand how the significance of this plot an example is given as follows. The transfer function is modelled after a gaussian with amplitude 1 and standard deviation of 0.2 as follows. Here one can think of the Rubidium transition frequency to be centred to the 0 point.

$$R(\omega) = 1 - e^{-\frac{\omega^2}{2(0.2)}} \quad 4.5$$

Following this, we can obtain $\chi(\omega)$ to be as follows, as described above. Here the sidebands are taken to be 0.5Hz away from the carrier frequency.

$$\begin{aligned} \chi(\omega) &= R(\omega)R^*(\omega+\omega_m) - R^*(\omega)R(\omega - \omega_m) \\ &= \left(1 - e^{-\frac{\omega^2}{2(0.2)}}\right) \left(1 - e^{-\frac{(\omega+0.5)^2}{2(0.2)}}\right) \\ &\quad - \left(1 - e^{-\frac{\omega^2}{2(0.2)}}\right) \left(1 - e^{-\frac{(\omega-0.5)^2}{2(0.2)}}\right) \end{aligned} \quad 4.6$$

We obtain a plot as follows in Figure 12, where the red plot represents the transfer function, and the blue plot represents ω vs $\chi(\omega)$. This plot of ω vs $\chi(\omega)$, otherwise also known as the error signal, is what allows for a PID response.

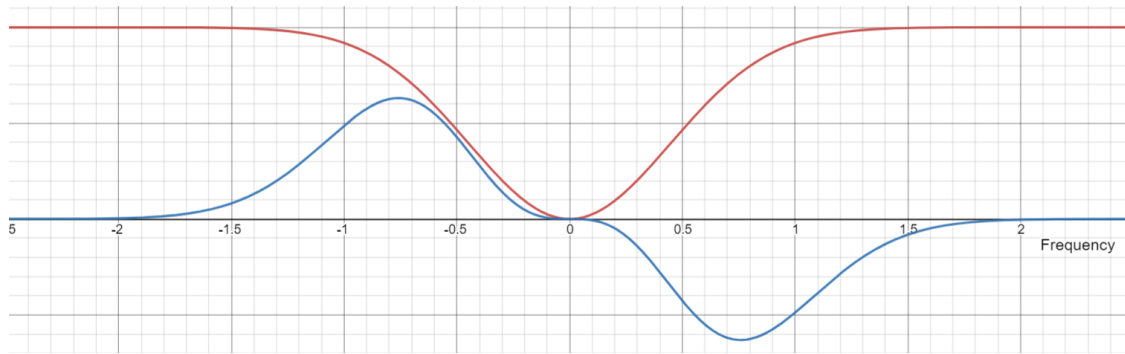


Figure 12: Calculate plot of example transfer function (red) and its error signal (blue). Transfer function represents the intensity of light that is incident on photodetector in the Pound-Drever Hall set-up. Frequency scale is relative to transition frequency of ^{87}Rb . At the transition frequency (at frequency=0 on plot), transfer function is at a minimum. Corresponding error signal (blue) has zero point at transfer signal minimum. Error signal is a slope along the 0 point that rises in one direction (left) and falls in the other (right). Based on this plot, PID feedback can be set-up to try to keep error signal value at 0, keeping beam locked to transition frequency.

After scanning through a range of frequencies and using the mixing process described to measure $\chi(\omega)$, this error signal is obtained, following which the carrier signal is adjusted such that the midpoint of this error-signal is at the zero point, i.e., a Rubidium transition frequency. At this point, one may stop scanning this range of frequencies, and measuring the $\chi(\omega)$ should be zero, as the carrier frequency is now at the transition frequency. At this point a PID feedback loop can be set-up to ensure that the value of $\chi(\omega)$ does not deviate from the zero point. This deviation is characterised by the error signal.

To scan a range of frequencies, a voltage with a ramp function profile of frequency 10Hz was applied onto the piezo, effectively allowing it to scan through a range of frequencies 5 times per seconds, with the amplitude of this voltage being proportional to the range size being scanned. This voltage was generated with the use of a function generator, and the error signal obtained from the mixing process is then observed on an oscilloscope. This error signal has been obtained for a beam from the LD808 diode centred on a 795nm $F=2 \rightarrow 1$ transition for Rubidium as shown in Figure 13.

PDH Error Signal at 795nm vs Frequency detune

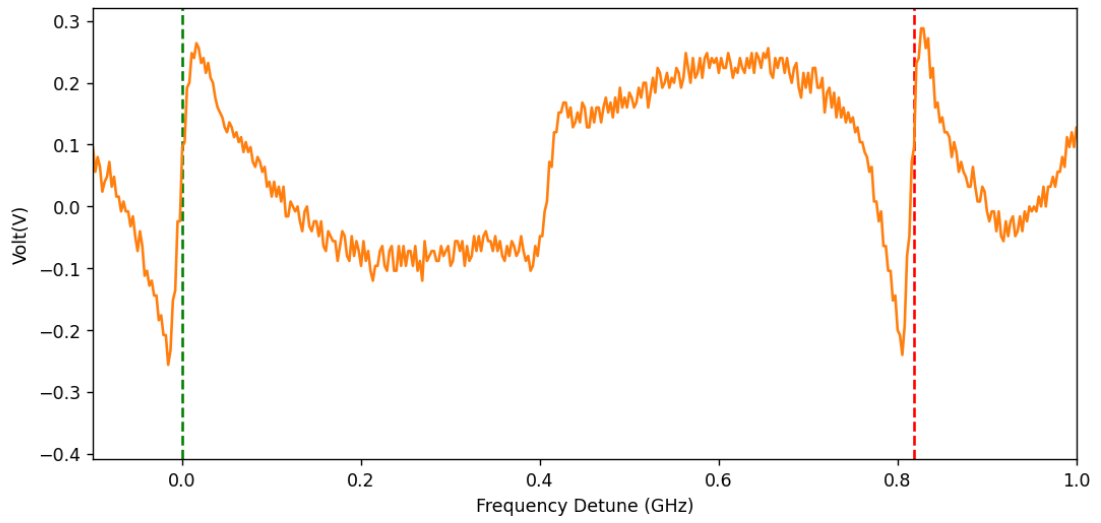


Figure 13: Plot of error signal at 795nm transition for ^{87}Rb , green dotted line (left) indicates the frequency at which $5S_{1/2}, F=2 \rightarrow 5P_{1/2}, F=2$ transition occurs, and the red dotted line indicates the $5S_{1/2}, F=2 \rightarrow 5P_{1/2}, F=1$ transition. The energy of these transmissions match that of a signal photon and laser photon respectively in the Six-Wave Mixing experiment

5 Fabry Perot Cavity

With reference to the six-wave mixing scheme, there are three wavelengths in play that are within 10GHz separation from each other, one of which is from a laser source at 377.104 391 THz, and the other two being emitted photons as part of the six-wave scheme at 377.111 222 THz and 377.105 205 THz. The laser is estimated to have a photon count 12 orders greater than that of the emitted photons. And so, the objectives to be met working towards a photon triplet source is to investigate if a Fabry-Perot cavity could be used to attenuate the photon counts from the laser, while preserving as many emitted photons as possible, and if so, investigate how many orders the cavity could suppress the laser by.

	Frequency
Generated photon	377.111 222 THz
Excitation Laser	377.104 391 THz
Generated photon	377.105 205 THz

A Fabry Perot cavity is a cavity that in a simplified view consists of two mirrors with a transmission and reflection coefficient. These cavities are used to filter out certain frequencies of light, by allowing only frequencies that are resonant with the cavity to pass through. In this section, the theory behind the Fabry Perot cavity and the optimal design parameters required to allow transmission of a particular frequency will be discussed.

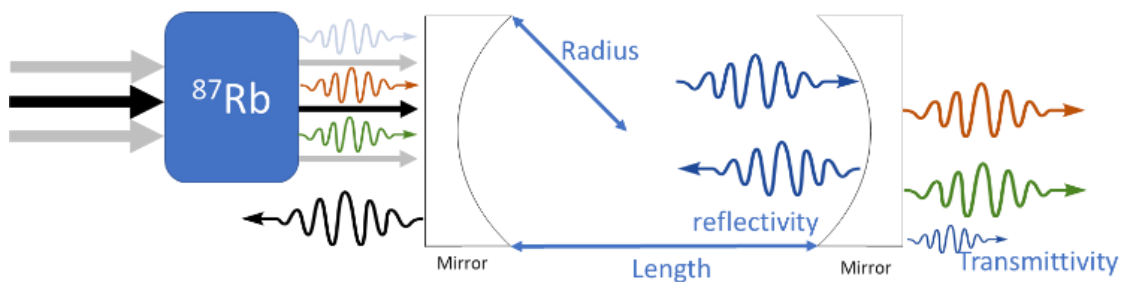


Figure 14: Fabry Perot Cavity separating generated photons and laser photons. Wavelengths resonant with cavity are transmitted and non-resonant wavelengths are reflected away. Factors of a cavity that affect the transmittivity of a wavelength are length of cavity, radius of mirrors, and reflectivity/ transmittivity coefficients of mirrors

A Fabry-Perot cavity can be characterized by the following properties, the length of the cavity or the distance between the mirrors, the radius of curvature of the mirrors, and

the reflectivity and transmittivity of the mirrors. These physical properties of the cavity determine the transmittivity of wavelengths, and also the gaussian mode that is allowed to exist within the cavity as well as stability of the cavity.

A stable cavity ensures that the beam size does not grow within the cavity and expand beyond the mirrors size, leaving the cavity, but also returns back to its original form after a reflection between both mirrors. This criterion for stability in cavities is characterized by the g-factor for each mirror, where L is the cavity length and R is the radius of the mirror

$$g = 1 - \frac{L}{R} \quad 5.1$$

The stability of a cavity is further given by the product of the g-factors for the two mirrors, $0 \leq g_1 g_2 \leq 1$ where 0 is the most stable configuration. In this case the g factor is 0 as L and R are the same in a confocal cavity.

With the assumptions that the beam has a gaussian profile, it is found that the equation for frequencies that can exist in a resonator cavity is as follows [23].

$$v_{qmn} = \frac{c}{2L} \left[q + \frac{1}{\pi} (m + n + 1) \cos^{-1} \sqrt{g_1 g_2} \right] \quad 5.2$$

Building on variables introduced, in this equation, c is the speed of light, q is the longitudinal mode of the wave in the cavity, while m and n are transverse modes associated with the intensity profile of the beam. For this discussion, it shall be assumed that the beam will be in its fundamental TEM₀₀ mode (m, n=0), and that only mode number q is being varied.

From the earlier equation obtained, the free spectral range (FSR) of the cavity can be calculated. The FSR is the frequency difference between the $q = x$ and $q = x + 1$ frequencies in a cavity, which from the earlier equation can be easily obtained to be as follows

$$v_{FSR} = \frac{c}{2L} \quad 5.3$$

The transmission intensity of a resonator is given by following equation, which can be derived from the Airy formula [24]([Vol. 179, Chap. 1, pp. 1 – 60.) In this equation, t_1, t_2 and r_1, r_2 are the two mirrors transmission and reflection coefficients, I_0 is the intensity of the incident beam on the cavity, and $\Delta\nu$ is the difference between the closest allowed frequency and the frequency of the incident beam.

$$I_t(\Delta\nu) = \frac{t_1 t_2}{(1 - \sqrt{r_1 r_2})} \frac{I_0}{1 + \frac{4\sqrt{r_1 r_2}}{(1 - \sqrt{r_1 r_2})^2} \sin^2\left(\frac{\pi\Delta\nu}{\nu_{FSR}}\right)} \quad 5.4$$

This allows for the graphing of the transmission vs frequency profile of the output light beam as shown in Figure 8. It is to be noted that the transmission is simply given by $I_t(\Delta\nu)/I_0$. With reference to Figure 8, the frequency difference between transmission peaks is the FSR frequency, and with a lower reflectivity coefficient, the full width half maximum (FWHM) frequency range increases. Since the objective of the Fabry Perot cavity is to allow transmission of one frequency and ensure minimal transmission for another, one may try to optimize parameters such as cavity length, radius of mirrors and reflectivity in order to ensure that the frequency for transmission is at a peak and is an allowed frequency, while the frequency to be blocked is at a transmission minimum in the cavity.

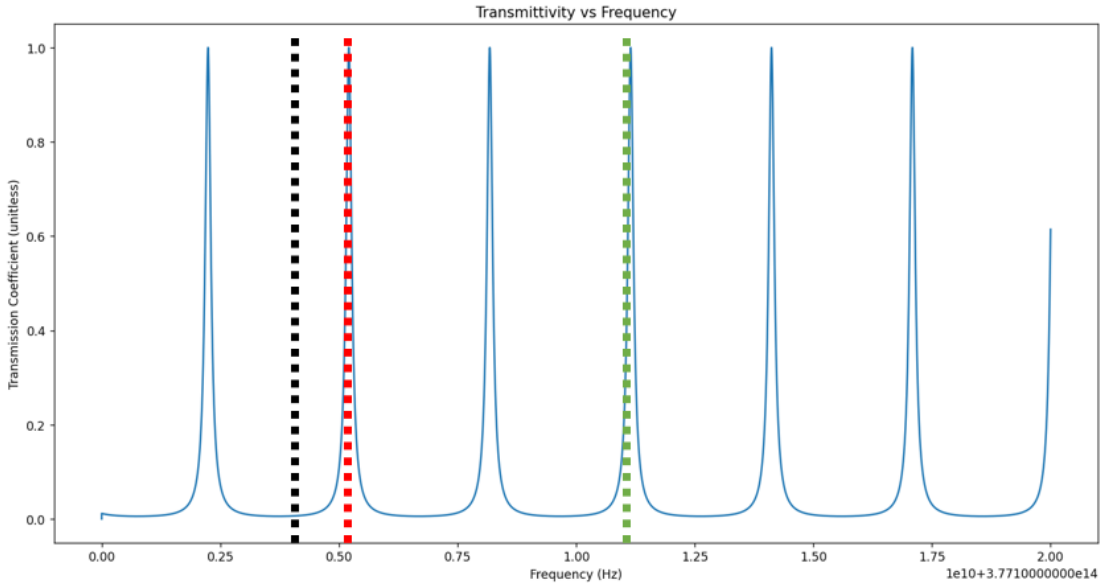


Figure 15: Simulation of Fabry-Perot cavity transmission profile with respect to six wave mixing experiment. Vertical dashed lines represent the three frequencies in six-wave mixing scheme at 795nm to be separated via a cavity; black represents input laser frequency, orange and green represent generated photons. Laser is to be attenuated and separated, hence close to a minimum on plot, generated photons to be transmitted via cavity, hence at a maximum on plot

6 Designing a Fabry-Perot Cavity

In this section, the physical parameters of components required to build a Fabry-Perot Cavity required to attenuate the laser with a frequency of 377.104 391 THz and transmit photons with frequency 377.105 205 THz will be investigated. These parameters are namely the length of the cavity, the radius and the reflectivity of the mirrors in the cavity, as well as the focal length and distance from cavity of a lens required to make an incoming gaussian beam match the cavity mode.

6.1 Length of Fabry-Perot Cavity

As mentioned in the previous section, the goal of designing a Fabry Perot cavity for this SWM experiment is to attenuate the laser with a frequency of 377.104 391 THz and transmit photons with frequency 377.105 205 THz. In order to do so, the cavity must be first designed such that the transmission peak lies on the photon's frequency and the laser's frequency lies on a transmission minimum. By definition, the Free-Spectral Range (FSR) is the difference in frequency between two peaks, and so a simple way to determine what this FSR should be for the designed cavity is to have it be twice the difference between the laser and photon frequency. That way, the photon transmission can be adjusted to be at a peak and the laser's transmission can be at a minimum in between two peaks. By manipulating the formula for $\nu_{FSR} = \frac{c}{2L}$ (Eqn. 5.3), we can find that the desired length for this cavity should be as follows (Eqn. 7.1). This gives a value for cavity length to be 0.092074cm.

$$L = \frac{c}{4 * (\nu_{Pump} - \nu_{Photon})} \quad 6.1$$

The cavity would also need to have some degree of stability in terms of length. A small change in the cavity's length, be it from mechanical noise or temperature, can potentially take the cavity off resonance with the desired transmission frequency of 377.105 205 THz. To find out how the precision of the length needs to be, one must find the FWHM frequency for the cavity, given by Eqn. 6.2. As previously explained, the Fabry-Perot cavity can transmit certain frequencies of light dependent on the ν_{FSR} where there is peak transmission through the cavity. The FWHM frequency of a cavity refers to the frequency range between the 50% transmission strength regions around this peak. In order to find the precision of length required, Eqn. 6.2 was manipulated with the substitution $\nu_{FSR} = \frac{c}{2L}$ (Eqn. 5.3) being made. The FWHM should encompass the

bandwidth of generated photons (20MHz), and so with that substitution, the corresponding accuracy of L was determined to be on the order of microns.

$$\Gamma^{FWHM} = \frac{v_{FSR} * (1 - r)}{\pi\sqrt{r}} \quad 6.2$$

6.2 Reflectivity of Mirrors in Fabry-Perot Cavity

The next step in the design process is determining what reflectivity of mirrors (r) to use. This is dependent on the bandwidth of the generated photons (20MHz). Ideally, the bandwidth of the generated photons should fall within the FWHM range of the cavity's transmission peaks spectrum. This FWHM frequency is given by the equation as follows (Eqn. 6.2).

By varying reflectivity r in Eqn. 6.2, we can determine if the FWHM bandwidth matches the photon bandwidth of 20MHz. It was found that mirror reflectivity lower than 0.97 was suitable enough to meet this criterion. However, the goal is to attenuate the laser's frequency as strongly as possible, and it is also found that the higher the reflectivity of the mirrors, the smaller the FWHM bandwidth of the cavity is and the greater the attenuation off resonance will be. Hence, the highest allowable value for reflectivity, 0.97, was chosen for the mirrors.

6.3 Radius of Mirrors in Fabry-Perot Cavity & Focusing Lens Parameters

In designing a Fabry-Perot cavity, the last variable to consider is the curvature of the mirrors. The mirrors to be used are circular mirrors and their radius of curvature determines the shape that a beam will take within a cavity. This section of the design process is required to determine how a collimated beam can be focused into a cavity to enter such that the beam does not diverge within the cavity. With the assumption that the beam entering the cavity is a gaussian beam and that the cavity is stable (beam does not diverge within the cavity), it can be found that the beam can only take on one particular gaussian mode within the cavity. In order to calculate what this mode will be, the following steps can be taken.

Gaussian beams can be characterized by a Q-factor, which contains information regarding the beam's properties such as beam diameter, the beam waist and its position, and the curvature of the beam wavefronts. When a gaussian beam passes through an

optical system, the beam shape can change, and this beam evolution is given by the ABCD law. In this law, the ABCD matrix of the optical components the incoming beam interacts with is determined and the following equation is used to evolve a beam with q-factor q_1 into q_2 after interacting with the optical system characterized by the ABCD matrix.

$$q_2 = \frac{A * q_1 + B}{C * q_1 + D} \quad 6.3$$

In the case of a stable cavity, consider a round trip in the cavity starting from one mirror surface. For the cavity to be stable, the beam should return to its original shape after one round trip within the cavity, and so q_2 can be substituted as q_1 . One finds that this manipulation gives a quadratic equation that can be solved to find q_1 , the beam profile at one of the mirror surfaces of a stable cavity, which gives the following equation.

$$q_1 = \frac{(A - D)}{2C} \pm \frac{\sqrt{(D - A)^2 - 4B * C}}{2C} \quad 6.4$$

Next, the ABCD matrix for one round trip within a cavity should be determined. This round trip starts with propagation to the next mirror, reflection at the mirror, propagation back to the first mirror, and reflection off the first mirror to complete the round trip. This ABCD matrix is given as such.

$$\begin{aligned} \begin{pmatrix} A & D \\ B & C \end{pmatrix} &= \begin{pmatrix} 1 & 0 \\ -\frac{2}{R_1} & 1 \end{pmatrix} \begin{pmatrix} 1 & d \\ 0 & 1 \end{pmatrix} \begin{pmatrix} 1 & 0 \\ -\frac{2}{R_2} & 1 \end{pmatrix} \begin{pmatrix} 1 & d \\ 0 & 1 \end{pmatrix} \\ &= \begin{pmatrix} 1 - \frac{2d}{R_2} & 2d - \frac{2d^2}{R_2} \\ -\frac{2}{R_1} - \frac{2}{R_2} + \frac{4d}{R_1 * R_2} & \frac{4d^2}{R_1 * R_2} + 1 - \frac{4d}{R_1} - \frac{2d}{R_2} \end{pmatrix} \end{aligned} \quad 6.5$$

Substituting the values for length of cavity as distance of propagation, and the radius of curvature for both mirrors, one can find the numeric value of the ABCD matrix, and then sub these values into the quadratic solution for q_1 to determine the profile of the gaussian beam that exists within the cavity. It is to be noted that in this process, the curvature of mirrors is an independent factor and hence their values are

chosen based on availability instead of exact calculations, unlike cavity length and mirror reflectivity.

From the value of q_1 obtained for the chosen values of mirror radius of curvatures, one can now determine what optics should be used to focus a collimated gaussian beam into a cavity such that the beam entering the cavity at a mirror's surfaces also has a gaussian q-factor matching q_1 . Approximating the incoming beam as a collimated gaussian beam q_0 , the q-factor of such a collimated beam can be given as $q_0 = \frac{i\lambda D^2}{\pi}$, where D is the diameter of the collimated beam. The diameter can be further approximated to be that of a beam from a single mode fiber collimated by an aspheric lens, given by $D = 2 * NA * F$, where NA is the numerical aperture of the fiber and F is the focal lens of the aspheric lens.

The objective is to now find a suitable lens that can be used to evolve the beam q_0 into q_1 . The ABCD matrix of such a system will now comprise of a lens with some focal length, followed by some distance of propagation, followed by a cavity mirror, which can be approximated as a thick lens. For ease of calculations, this matrix was broken into two segments, the focusing lens with some distance of propagation, and a matrix representing the cavity mirror as a thick lens. First, the ABCD matrix for a Plano-concave cavity mirror was determined, and this was found to be as follows, where n , T and R is the refractive index, the thickness, and the radius respectively of the mirror.

$$ABCD_{Mirror} = \begin{pmatrix} 1 & \frac{T}{n} \\ \frac{n-1}{R} & \frac{nR + T(n-1)}{nR} \end{pmatrix} \quad 6.6$$

By performing an inverse operation on this matrix and applying the ABCD law on q_1 , one can find the q-factor of a beam just about to enter the Plano-concave mirror, which shall be referred to as q . The mathematical operations performed are as follows.

$$ABCD_{Mirror}^{-1} = \begin{pmatrix} \frac{nR + T(n-1)}{nR} & \frac{-T}{n} \\ \frac{1-n}{R} & 1 \end{pmatrix} \quad 6.7$$

$$q = \frac{\left(\frac{nR + T(n-1)}{nR}\right) q_0 - \frac{T}{n}}{\left(\frac{1-n}{R}\right) q_0 + 1} \quad 6.8$$

The ABCD matrix for a lens with focal length f is given as follows, $ABCD_{lens} = \begin{pmatrix} 1 & 0 \\ -\frac{1}{f} & 1 \end{pmatrix}$. From this, the q-factor of the beam q_{len} , having evolved from q_0 after a lens can be given by the ABCD law as follows.

$$q_{len} = \frac{q_0}{-\frac{q_0}{f} + 1} \quad 6.9$$

Recalling that q_0 takes on the form $q_0 = \frac{i\lambda D^2}{\pi} = iz_0$, where z_0 is a real positive number, this equation governing q_{len} can be further manipulated to take the following form.

$$q_{len} = \frac{-z_0 f}{f^2 + z_0^2} + i \frac{z_0 f^2}{f^2 + z_0^2} \quad 6.10$$

From this form, it can be seen that the q factor can be split into its real and imaginary components as both z_0 and f are real values. As per the gaussian beam description obtained from the q-factor, the real part of q_{len} represents the displacement of the beam's location with reference to its beam waist, and the imaginary component of q_{len} relates to the beam-waist of the beam via the following equation.

$$Im[q_{len}] = \frac{z_0 f^2}{f^2 + z_0^2} = \frac{\pi \omega_0^2}{\lambda} \quad 6.11$$

Once this form has been obtained, the following two constrains can now be implemented. The first being that the beam waist for both q_{len} and q should be the same, since they are supposed to be identical beams, just one having propagated some distance d . The second is that their beam waist should be situated at the same location based on both q-factors.

From the first constrain, it can be seen that for both q_{len} and q to have the same beam waist, their imaginary components must be identical to each other, and hence the focal length f of the focusing lens can be calculated as such.

$$Im[q] = Im[q_{len}] = \frac{z_0 f^2}{f^2 + z_0^2} \quad 6.12$$

$$f = \sqrt{\frac{z_0^2 * Im[q]}{z_0 - Im[q]}} \quad 6.13$$

From the second constrain, the distance between the focusing lens and the cavity mirror can be found to be as given.

$$d = Re[q_{len}] - Re[q] \quad 6.14$$

The mirrors that were selected were Plano-concave mirrors with radius $R = 0.1$, and the collimated beam that was to be focused into the cavity had a beam diameter of about $\sim 1.1\text{mm}$. Based on these initial conditions and the imposed constrains, the focal length required of the focusing lens and ideal distance between the lens and the first incident cavity mirror are calculated to be 0.424m and 0.376m , but considering availability, a lens with focal length 0.4m was selected, with an adjusted distance of $\sim 0.35\text{m}$.

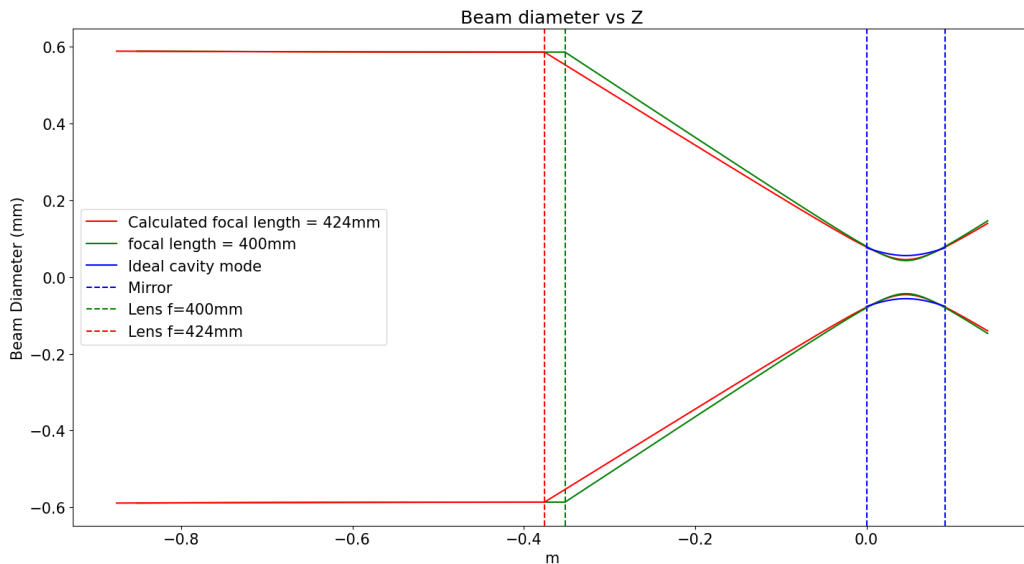


Figure 16: Plot showing the beam diameter of a collimated beam passing through a lens and matching the mode inside a cavity. Red and green dotted vertical lines represent position of 424mm and 400mm focal length lenses, and blue dotted vertical lines represent the position of mirrors of the cavity. Blue solid lines indicate the ideal cavity mode of a stable cavity.

And with these numbers obtained, a Fabry-Perot cavity can now be built with the numbers obtained in the design process. For optical components, the mirrors required will be of radius 0.1m with reflectivity of 0.97% , and in addition, a lens with focal length of 0.4m will be required to focus the beam into the cavity such that the incoming beam matches the cavity mode. For the scale in terms of distance, the set-up

needs to be built such that the spacing between cavity mirrors is about 9.2cm, and the distance from the cavity to the focusing lens is about 0.35m.

7 Fabry-Perot Cavity Set-up

In this segment, the Fabry-Perot set-up is discussed in greater detail. These would include the structure and components that made this cavity, as well as how this cavity was aligned and then locked to a resonant wavelength.

7.1 Cavity build

With the simulations done in Chapter 6, the necessary mirrors and focusing lenses were obtained. The mirrors used were 0.97% reflectivity Plano-Concave mirrors, with a physical diameter of 0.5". As per Chapter 6, the length of such a cavity would be approximately 9.2cm. Another consideration was that the length of this cavity would need to be accurate and stable to a length of sub-microns, and so by mounting one of the mirrors on a ring piezo, this length could be controlled to a precision of sub-microns. This accuracy and precision of the cavity length was achieved by using a mount as shown in Figure 17, where one mirror was mounted on a fixed end with a piezo, and another was mounted on a sm05 tube containing the second mirror screwed into the mount. The Plano-concave mirrors are mounted such that the concave surface is facing the inside of the cavity.

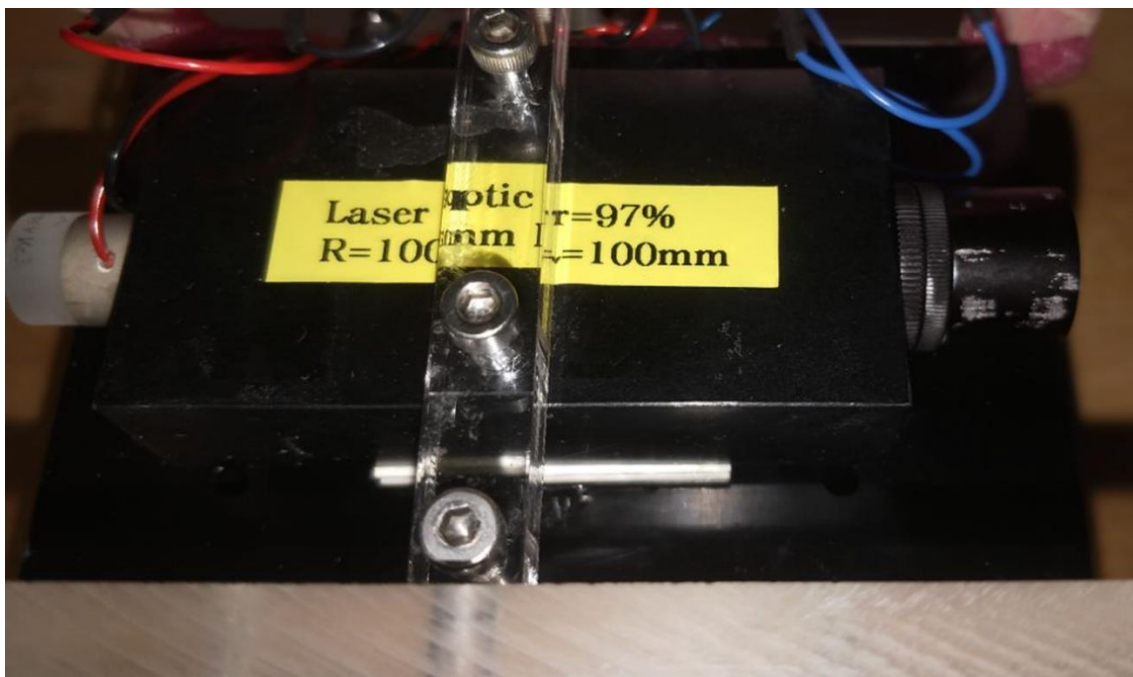


Figure 17: Fabry-Perot Cavity mount. One mirror mounted on a piezo fixed to the mount (left) for fine sub-micron cavity length adjustment, one end mounted in SM05 tube for coarse length adjustment, with tube adjustable to 0.1mm precision using vernier callipers.

The mount itself is a rectangular block with a hollow cylindrical cavity with sm05 threading to allow for sm05 tubes to be screwed into the mount. This set-up now allowed for the length to be controlled by coarse adjustments on the order of sub-millimetres of the sm05 tube attached to the mount, as well as fine adjustments via the piezo on the order of sub microns. It is to be noted that this cavity only has one degree of freedom, which is the length of the cavity itself, in the direction of propagation of light. The angle that the mirrors make with the optical axis were taken to be near perpendicular and assumed to have minimal impact on the transmission profile at small deviations from normal incidence.

7.2 Cavity alignment setup

In order for a Fabry-Perot cavity to have maximum transmission, the incident beam must align with the optical axis of the cavity. This would mean that the incident beam must enter the cavity at normal incidence, and through the centre of the incident mirror. As such, in order to take an incoming beam and feed it into a cavity through its centre at normal incidence, two mirrors will be required to control these two degrees of freedom; the first being angle of incidence and the second being the x-y position of the beam with respect to the centre of the cavity.

From Chapter 6, it can be seen that apart from the cavity itself, a focusing lens would be required to direct the incoming beam from a single mode fibre into a gaussian profile, and that it would have to be a certain distance away. Additionally, the beam should also pass through the lens at normal incidence and through its centre to prevent any beam distortion. In terms of alignment, this would mean that in order to adjust the distance between the focusing lens and the cavity, the lens should be mounted on a Z-translation stage. Additionally, another set of two mirrors should be used to ensure that the beam passes through the centre of the lens at normal incidence.

Finally, the beam that is being output from the single-mode fibre should be as collimated as possible, and so the aspheric lens used to collimate the beam output from a single-mode fibre was mounted on a z-translation stage. This ensured that the beam's collimation could be adjusted to improve the transmittivity through the cavity.

7.3 Cavity Alignment with Camera

In order to align the cavity, a monochrome CMOS Camera is used to view the beam profile after the cavity. The use of a single-mode fibre ensures that the beam is gaussian with only the ground state transverse modes present. Using this camera allowed for

verification of the shape of the beam profile. Ideally, it should appear as a circular beam with only one bright spot in the centre, with no diffraction patterns such as rings, and this would indicate that there are no higher order TEM modes present within the cavity.

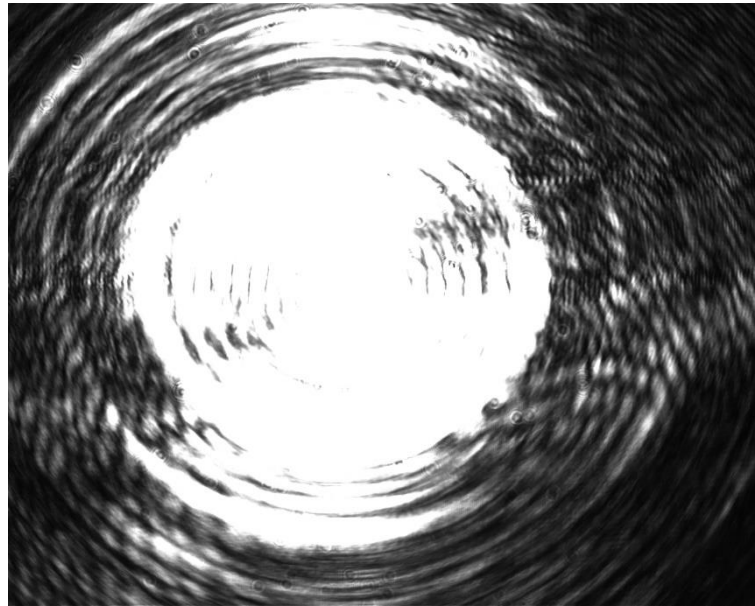


Figure 18: Image of beam obtained from monochrome CMOS Camera placed at the end of a Fabry-Perot Cavity. This stage is used for cavity alignment, where the objective is to alter the trajectory of incident light into the cavity such that image is circular in shape with minimal diffraction patterns, indicating normal incidence of beam with the cavity.

7.4 Cavity Alignment with Oscilloscope and ^{87}Rb Spectroscopy Signal

With the cavity coarsely aligned with a camera, the camera can now be replaced by a photodiode to measure the intensity being transmitted. The photodiode can now be used to plot an intensity of transmission through the cavity vs frequency plot. This would mean that the 795nm laser source being input into the cavity should scan a range of frequencies, as shown in Chapter 4 with the error signal trace. And so, with a plot of the error signal trace overlaid with the plot of transmitted intensity through cavity vs frequency, one obtains a Figure as shown in Figure 19.

Error Signal and Transmission profile vs Frequency

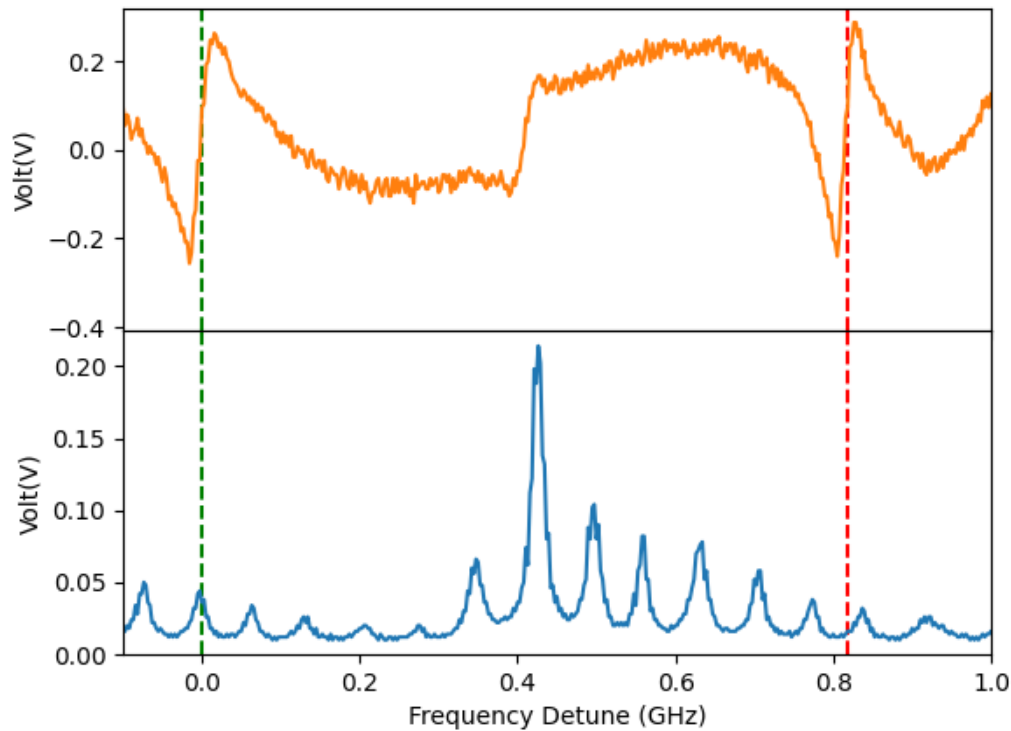


Figure 19: Error Signal and Transmission profile through a detuned Cavity vs frequency overlaid together. X-axis is frequency detune from the frequency that the cavity needs to transmit. The top plot shows ^{87}Rb spectroscopy in the 795nm regime. Refer to Figure 13 for details on top plot. Bottom plot shows transmittivity vs frequency detune, with vertical green and red lines showing regions where the transmission profile should be a maximum and minimum respectively.

It is to be noted that the 0GHz frequency detune point is the frequency that the cavity should be locked to (indicated by green vertical line). Additionally, the objective is to attenuate another frequency detuned by about 0.8GHz (indicated by red vertical line). As can be seen from the Transmission profile vs Frequency plot, there are two undesired features in this plot.

1. The maximum possible peak transmission occurs at a detuning approximately 0.4GHz away. This means that the cavity length needs to be adjusted for the highest possible peak to occur at the 0GHz detune point.
2. There are multiple peaks that can be observed in the transmission vs frequency plot. These peaks are higher order TEM modes, which indicate an imperfect alignment of the cavity.

To rectify these two problems, a bias voltage is applied to the cavity piezo, which results in sub-micron adjustments of the cavity length, and hence allowing to shift the highest possible transmission peak to the 0GHz detune point. To fix the alignment with

the cavity and minimise the TEM modes, further manipulation is done to optimise the angle and tilt of the mirrors, the z-translational position of the focal lens as well as the z-translation of the aspheric lens used to collimate the beam output from a single mode fibre. By adjusting these variables, the following transmission profile was achieved, shown in Figure 20. As can be seen from this figure, the peak transmission is still offset from the frequency that is to be used to lock the cavity (green vertical line). This final offset is to be rectified via Pound-Drever Hall locking of the cavity.

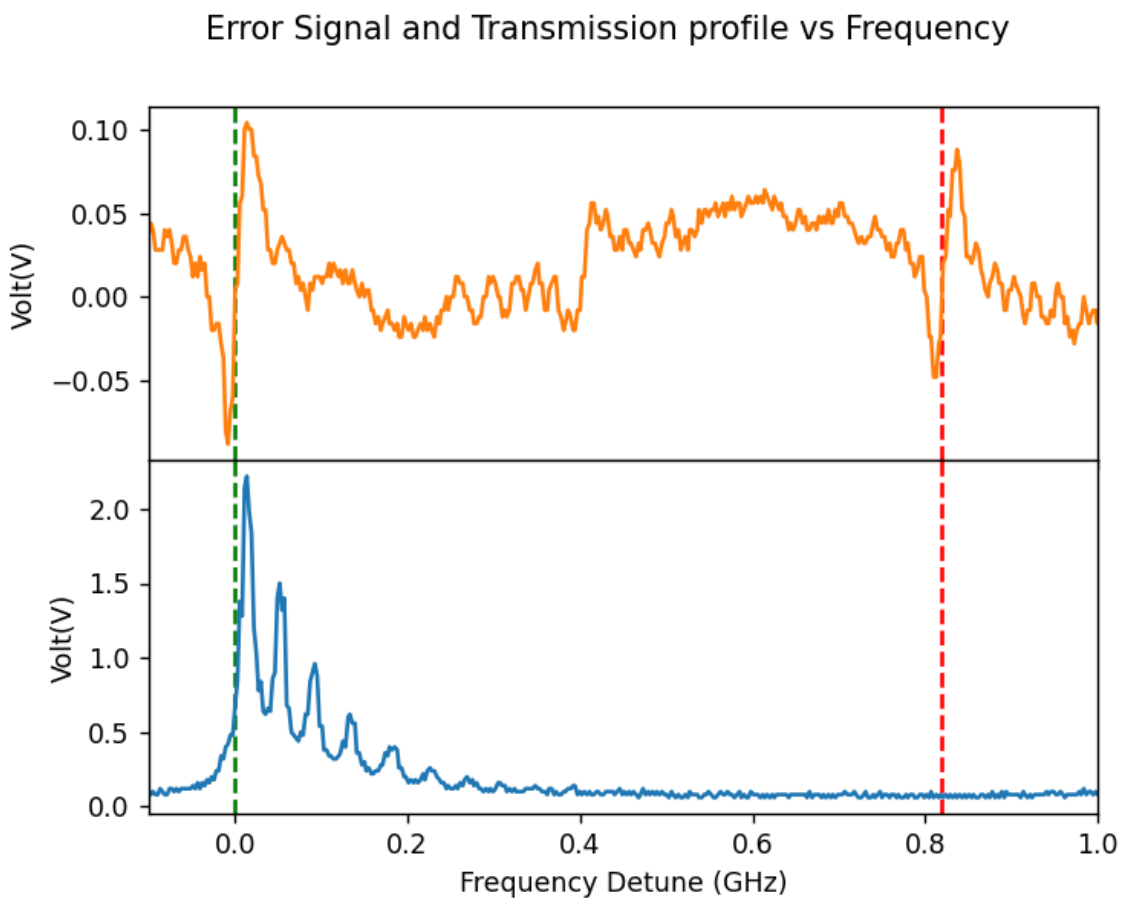


Figure 20: Error Signal and Transmission profile through a tuned Cavity vs frequency overlaid together. With reference to figure 19, transmission profile is close to maxima and minima respectively at green and red vertical lines. Pound-Drever Hall locking can be now performed on Cavity to align transmission maxima with atomic transitions of ^{87}Rb .

7.5 Pound-Drever Hall Locking of Cavity

Once the alignment of the cavity has been performed, Pound-Drever Hall locking can be done with relative ease. An aligned cavity would already mean that the beam being reflected off the cavity is traversing the same beam path as the incoming beam into the cavity, due to alignment being the beam incident on the cavity mirrors. As described in Chapter 4, Pound Drever Hall locking is done by using an Electro-Optical

Modulator (EOM) to add additional sidebands to the dominant frequency output from the single-mode fibre. A polarising beam splitter combined with a quarter wave plate is used to ensure that the reflected beam will be separated from the incident beam at the polarising beam splitter, which then allows for the reflected beam to be focused into a transimpedance amplifier to produce an error signal. The process via which this signal is manipulated from the transimpedance amplifier into an error signal has been explained in Chapter 4, and so its explanation will be omitted in this section.

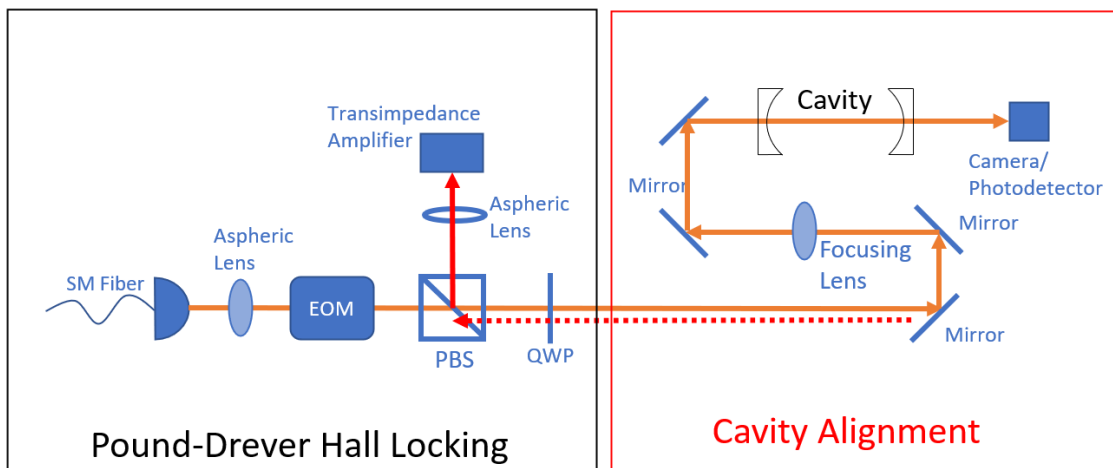


Figure 21: Schematic of Set-up used to align and perform Pound-Drever Hall (PDH) Locking of the Fabry-Perot Cavity. Left box shows the set-up used to perform PDH locking, Right box shows set-up required to align beam with the cavity and focusing lens at normal incidence. Electro-Optical Modulator, PBS: Polarising Beam Splitter, QWP: Quarter Wave Plate.

7.6 Measurements and Results

Once the Fabry-Perot cavity had been locked to the desired Rubidium transition frequency, a powermeter was used to measure the transmission coefficient by measuring the intensity of the beams before and after the cavity. This measurement gave a transmission coefficient of 0.3, which is far from the desired transmission coefficient of 0.9. One can see why this is the case by referring to Figure 20, where there can be multiple smaller peaks seen beside the highest peak (Frequency cavity is locked to). These peaks are formed due to higher order TEM modes, and this means that the total energy of the beam is being split across these TEM modes, hence resulting in a lower transmission coefficient. These higher order TEM modes have most likely appeared due to imperfect alignment of the cavity. It is to be noted that this cavity only had one degree of freedom (Length of cavity) in the form of a z-translation, and so by adding tip-tilt functionality to the mirrors of the cavity the higher order TEM modes could have been suppressed.

The second property that was of interest is the max transmission to attenuation ratio. In this case, transmission is measured at the frequency of a generated photon, while attenuation is measured at the frequency of the laser source. This ratio was found to be 25. This number was expected to be approximately 2 orders as well, and as such, it is hypothesized that with a more robust cavity design this ratio can be maximised.

8 Outlook: Incorporating Fabry-Perot Cavity into Six-Wave Mixing

Simulation work done on Fabry-Perot cavities has shown that it is possible to use them for separation of the 795nm photons via narrow-band spectral filtering. An External Cavity Diode Laser (ECDL) has been built to emulate one of the generated photons to lock the cavity to. Following this a cavity was built to lock this ECDL, and its transmission coefficient for this ECDL as well as the transmission coefficients at a separate frequency (photon from laser source in Six-Wave Mixing meant to be separated) is measured.

The results obtained show that if this Fabry-Perot Cavity was to be used in the Six-Wave Mixing experiment, it would be able to attenuate the laser source's intensity by about 2 orders with respect to the generated photons intensity with a single cavity. However, the laser source's intensity is estimated to be about 12-13 times greater than that of the generated photons. As such it is estimated that about 5-6 such Fabry-Perot cavities will need to be used in series together. However, the cavity design will need to be improved upon to ensure greater transmittivity and to eliminate the presence of higher order TEM modes within the cavity.

The Fabry-Perot Cavities will have to be locked using a narrowband laser at the same frequency as the generated photons. However, during the Six-Wave Mixing experiment, when a measurement is being made of the generated photons, the locking laser will have to be turned off, and during this measurement period when the laser is turned off, the cavity will need to be stable enough to not detune from the required resonant frequency. This stability can be ensured by adjusting the PID controls that control cavity length using a piezo. The objective of these PID adjustments would be to ensure that the cavity does not go out of lock due to a fast PID response.

Additionally, the measurement should only take place after a short delay from when the locking laser is turned off. This delay is to allow for the light trapped within the cavity to dissipate. To determine how long this time delay should be, one needs to refer to the cavity ring-down time, which is the time required to light intensity within the cavity to drop to $1/e$ of its initial intensity. Depending on the power of the locking laser, sufficient time must be given to allow the photon count from the locking laser to drop below the generated photon count (estimated to be 500 counts per second).

9 Appendix 1: Optical components

In this section, the optical components that are used in this project is introduced. These components are required for both the laser locking and the Fabry-Perot cavity building process. The components used were all mounted with appropriate mounts and screws onto an optical table. At this junction, the description of what these optical components do will be given instead of a discussion on their function in the project.

9.1 Polarisers

Polarizers are optical components that allow light in a certain linear polarization to pass through. They can be used to polarize unpolarized light or control the intensity of linearly polarized light that passes through it.

9.2 Mirror

Mirrors in optical labs are reflective surfaces characterized for use at a specific wavelength range, with typically a high reflective coefficient of 99.7% at the ideal wavelength. They are typically used to divert the beam path and with the help of a mirror mount make minor adjustments to the orientation of the mirror, allowing users to achieve coupling or achieve the desired beam path.

9.3 Beam Splitter (BS)

Beam Splitters are optical components that ideally have a surface with a reflective and transmission coefficient of 50% for unpolarized light. Incident light that hits this surface is able to hence divert into two paths, one reflected and one transmitted. There are two types of beam splitter, non-polarizing beam splitters (NPBS) and polarizing beam splitters (PBS). NPBS can split light unpolarized or polarized into two beam paths with 50% in each path, whereas PBS allows a certain linearly polarized light, conventionally horizontally polarized light, to transmit and an orthogonal polarization, conventionally vertically polarized light, to reflect off the surface, a property which allows the user to choose the intensity of transmission between both optical paths by varying the linear polarization of the incident beam. Both types are typically characterized for use in a certain ideal wavelength range.

9.4 Wave Plate

Wave plates are optical components that are made of a birefringent crystal. Birefringence refers to the property of a material having varying refractive indexes along different linear polarizations paths of an incident beam. With respect to wave plates the polarization with the lowest refractive index is the fast axis and the polarization with the highest refractive index is the slow axis, and due to this property, incident polarized light experiences a phase shift difference for components its fast axis and slow axis. Wave plates are also frequency dependent as different frequencies will experience different phase differences in polarization components for the same polarization.

The two most common types of wave plates are Half Wave Plates (HWP) and Quarter Wave Plates (QWP). HWP introduce a phase difference of $\lambda/2$ between the slow and fast axis, which can be used to rotate the linear polarization of a polarized light from one orientation to another. QWP introduce a phase difference of $\lambda/4$ between the slow and fast axis, allowing linearly polarized light to be evolved to an output circularly or elliptically polarized light.

9.5 Acousto-Optic Modulator (AOM)

The Acousto-Optic Modulator is a device that contains a crystal attached to a piezo-electrical transducer. This allows for the device to use the acousto-optic effect to diffract and shift the frequency of light by using a RF acoustic wave to periodically change the refractive index of the crystal, effectively forming a diffraction grating. This allows one to control the frequency and direction of the output light. The $m=\pm 1$ modes of the diffracted beam are at frequencies $\nu \pm \nu_{RF}$, with ν being the incident frequency, and ν_{RF} being the RF signal frequency.

9.6 Electro-Optic Modulator (EOM)

The Electro-Optic Modulator is a device that applies an electric field within a crystal which oscillates the refractive index of the crystal via a RF electric signal. This results in modulation of the input beam by the addition of sidebands to the frequency profile of the incident beam, with the sidebands being at a $\nu \pm \nu_{RF}$, with ν being the incident frequency, and ν_{RF} being the RF signal frequency.

10 Appendix 2: Non-Optical components

In this section, devices and equipment that were used to supplement the project either as measuring devices or without being an optical part of the set-up is discussed and introduced.

10.1 Powermeter

The powermeter is an optical power measuring device that is used to measure the intensity of light incident on it. It does so with the use of photoresistors and by measuring the potential across them with a potential divider.

10.2 Optical Spectrometer

The optical spectrometer is a device used to measure the frequency spectrum of an input beam with an accuracy of $\pm 1\text{nm}$ from the real wavelength. The model used in this project is used to measure frequencies ranging from 720 to 850 nm.

10.3 Function Generator

The function generator in this project is used to generate sine waves at 22KHz used to power an EOM and a ramp function at 10Hz used as a reference signal for the Piezo. This device is used primarily for laser locking.

10.4 Oscilloscope

The oscilloscope is a device used to graphically display voltages and signals. In this project, it was used primarily to find error signals and perform laser locking.

10.5 Wave Meter

The wave meter is an interferometer-based measuring device used to measure the frequency of a beam up to a precision of MHz. This device was primarily used to verify that the ideal frequency has been achieved via the laser locking process.

10.6 Laser Driver

The laser driver is a printed circuit board that allows its user to connect to a computer, control and measure various properties of the laser and its housing unit, mainly the current being supplied to the laser diode, and the temperature of the laser diode.

10.7 FM Board

The FM Board is a printed circuit board with its function in this project primarily being to provide frequency modulation and a PID response to control the laser diodes frequency via the Pound-Drever Hall process.

11 Appendix 3: Six Wave Mixing Experimental Set-up

The experimental Set-up for the Four-Wave Mixing (FWM) and Six-Wave Mixing (SWM) experiment shall be briefly discussed in this section.

A collinear geometry has been selected for the SWM experimental set-up due to the advantage it provides over other orientations when it comes to calibration. This collinear geometry allows for the FWM set-up to be modified into a SWM set-up as well without needing to recalibrate the generated photon paths for collection by a detector or collimation into single mode fibres.

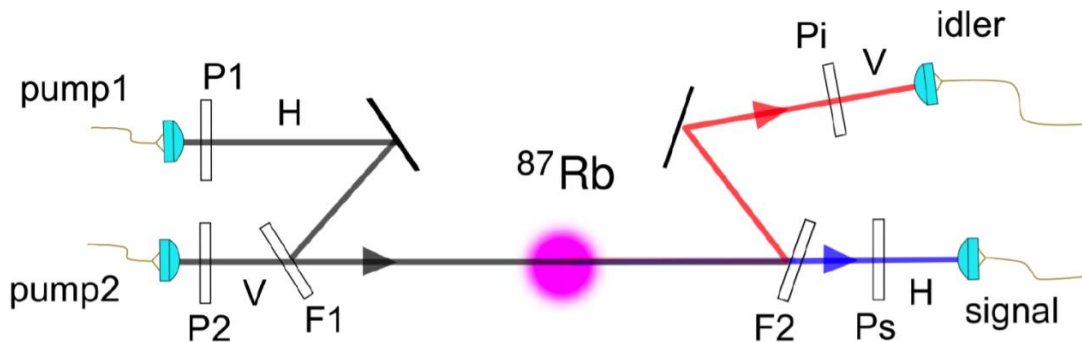


Figure 22: Four-Wave Mixing in ^{87}Rb cloud using collinear geometry[25]. Pump beams represented by black arrows of differing polarisations are combined using an interference filter. The two generated photons represented by red and blue arrows are then separated from pump beam using another interference filter, with polarisers P_i and P_s selecting the polarisation of the photons. Measuring dark and coincident counts between detectors can show entanglement between polarisations if the coincident counts are found to be substantially higher than the dark counts.

The FWM set-up is built before the SWM set-up. And so, with reference to FWM, the components required in the experimental set-up shall be explained.

11.1 Pump Laser

This category consists of the 780nm and 776nm pump lasers required for FWM. The building process and layouts for such lasers can be found in Chapter 3.

11.2 Magneto-Optical Trap

The Magneto-Optical Trap (MOT) is a vacuum chamber designed to trap an ^{87}Rb cloud in the centre of the trap. It conventionally has a magnetic field that grows linearly in strength outwards of the centre. This is achieved via anti-Helmholtz coils. The presence of this inhomogeneous magnetic field allows for trapping of the atoms in proper quantum states due to the Anomalous Zeeman Effect.

When the experiment is being conducted with the pump lasers, the magnetic field is momentarily shut off to ensure that Zeeman splitting does not affect the FWM/ SWM process by changing the energy levels of the hyperfine structure.

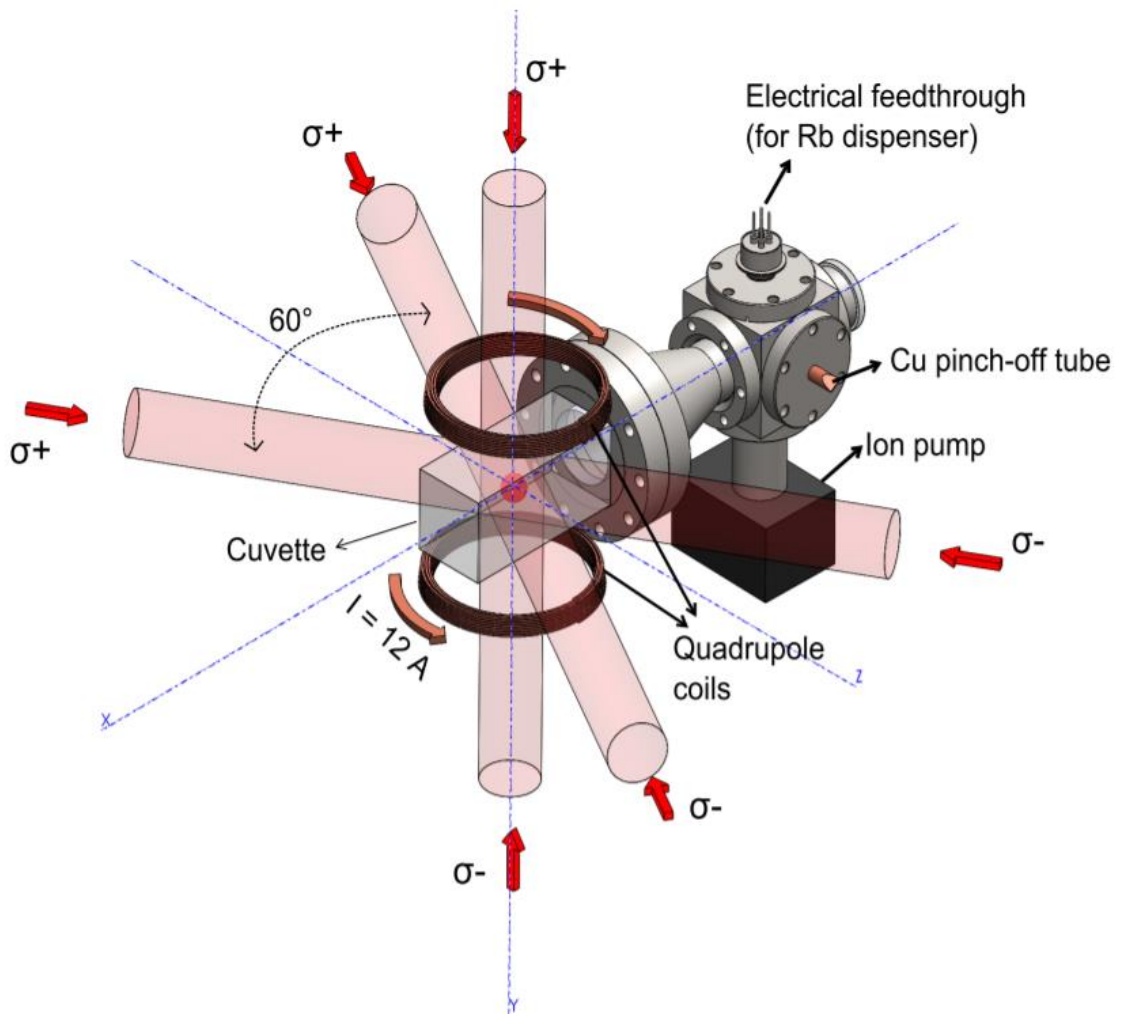


Figure 23: Set-up of the Magneto-Optical Trap (MOT)[26]. The Figure shows the vacuum chamber, with quadrupole anti-Helmholtz coils. Cooling beams are represented as red beams, with $\sigma+$ and $\sigma-$ representing the circular polarisations of the beams

11.3 Cooling Laser

The cooling laser is used to slow down atoms within the trap. This is achieved by having the cooling lasers be circularly polarised and red detuned from the ^{87}Rb $5S_{1/2}$, $F=2$ ground state transition. This allows for atoms with enough kinetic energy to absorb the red detuned photons, after which it can decay back to its ground state, thus losing its kinetic energy and being slowed in the trap.

Six such beams are oriented along the three cartesian x , y , z axis centred around the MOT, with two beams per axis pointing towards the centre of the MOT with opposing circular polarisations. The circular polarisation of these beams ensures that the cooling laser photons when absorbed/ scattered by an atom will push the atom back towards the centre of the trap. The mechanism for this is via Zeeman splitting through the MOT.

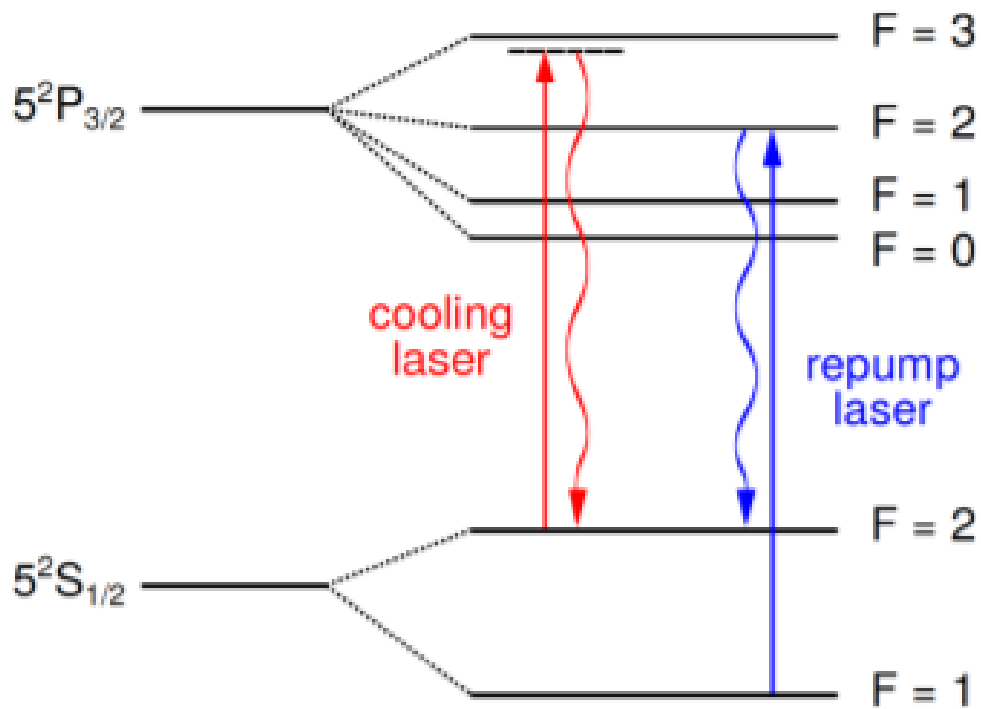


Figure 24: Hyperfine energy level of ^{87}Rb D2 line [25] with the target cooling and repump transitions

11.4 Repump Laser

Within the hyperfine structure of ^{87}Rb , there exists two $5S_{1/2}$ ground states, the $F=1$ and $F=2$ states. The FWM/SWM schemes require the preparation of the ^{87}Rb cloud in the $F=2$ ground state, and there is a small probability scattering from the $5P_{3/2}$, $F=2$ to the $5S_{3/2}$, $F=1$ state. These atoms cannot be cooled and will be unusable for the cyclic transitions of FWM/SWM. As such it is important to ensure that the ^{87}Rb atoms do not fall into the $F=1$ dark state. This is achieved by having a repump laser tuned to the $5S_{3/2}$, $F=1$ to $5P_{3/2}$, $F=2$ transition, via Raman Transitions.

11.5 Calibration Lasers (762nm and 795nm)

The calibration lasers are used to simulate the beam path of generated photons in these frequencies and to align the optical instruments required for the detection of these generated photons as well as filtering from the pump beams. It is to be noted that the

795nm calibration laser is to be used as a pump laser within the SWM experiment as well. The methodology to building these lasers can be found in Chapter 3.

It is to be noted as mentioned in Chapter 1, the objective of this project is to determine if photons can be generated via SWM. In specific, the project aims to find if 762nm photons can be generated via the SWM scheme. From Chapter 2, it is seen that three photons are generated via this scheme, one at 762nm and two at 795nm. These photons will have to be separated from the pump beams in this collinear geometry set-up, the pump beams being at 780nm, 776nm and 795nm. For the 762nm photon, this separation can be achieved via interference filters as the difference between the photon and pump frequencies is sufficiently large enough, on the order of THz. In the case of generated 795nm photons, separation becomes a challenge due to the photon frequencies and the 795nm pump frequencies being separated on the order of GHz.

Based on previous results from FWM[26], the pump beam (~35mW Sanyo diodes) was found to be 6 orders higher than the signal power from the generated photons (~80nW). Considering that the SWM is a $\chi^{(5)}$ process with lower photon counts than FWM which is a $\chi^{(3)}$ process, the pump beam power is expected to be minimally 6 orders of magnitude stronger than the signal photon power, the exact number of orders yet to be determined.

This would mean that the filtering techniques used to filter the 795nm pump beam and generated photons will need to not only require a narrow bandwidth, but also ensure that the pump beam can be attenuated to the point where the generated photon power is dominant over the pump beam power which is estimated to be about 12 orders higher. For this purpose of filtering, the use of a Fabry-Perot cavity was considered, with simulations performed to obtain the design parameters of such a cavity.

12 Appendix 4: Two-Photon Rubidium Spectroscopy

In the SWM scheme, a 762nm photon would be emitted, and this photon will need to be captured by a detector. With a collinear geometry for the experimental set-up as described in Chapter 5, the emitted photons from the SWM scheme will propagate in the same direction as the incoming pump beams. And so, a 762nm laser source would be required to calibrate the pathway from the MOT to a detector where 762nm photons can be detected. And with that motivation, this chapter will discuss how a 762nm laser source stabilised via PDH locking through two-photon Rubidium-87 spectroscopy was built, and some observations that were made when performing two-photon spectroscopy

12.1 Preparing ^{87}Rb at $5P_{3/2}$, $F=2$ state

The 762nm transition of ^{87}Rb is given by the $5P_{3/2}$, $F=2 \rightarrow 5D_{3/2}$, $F=2$ atomic transition, meaning to say that this is a transition for an excited state to another. And so, in order to perform this said transition, the ^{87}Rb atom needs to be prepared in the $5P_{3/2}$, $F=2$ state. This would additionally mean that an additional photon would be required to excite the ^{87}Rb atoms at ground state to this higher excited $5P_{3/2}$, $F=2$ state. For this purpose, in order to prepare ^{87}Rb atoms at the $5P_{3/2}$, $F=2$ state, a 795nm laser PDH locked via ^{87}Rb spectroscopy is used to excite ^{87}Rb atoms in a vapor cell. The process via which this laser was built, and frequency stabilised has been detailed in Chapters 8 and 9.

12.2 762nm External Cavity Diode Laser

The building process between the 762nm and 795nm sources do not differ, and it is to note that these ECDLs are identical in build. these two ECDLs, they use the same structural designs, similar laser drivers as well as the same laser diode; LD808. As such the specifications on how it was built is left out in this section and can be gleaned from Chapters 4 and 5. The only fundamental difference between these two ECDLs would be their output frequencies, which is a result of adjusting the diffraction grating's angle with respect to the incoming beam, as well as the temperature and current that the laser diode is operated at.

12.3 Rubidium Spectroscopy using 762nm source

To perform ^{87}Rb spectroscopy using a 762nm source, the 762nm beam is passed through the vapor cell, while ensuring that the beam overlaps the beam path of the 795nm beam. This ensures that the 762nm beam interacts with atoms that are in an

excited state. This meant that spectroscopy could only be performed with atoms excited by a 795nm photon, and that a higher population of excited atoms would result in a stronger spectroscopy signal. As such, the vapor cell was heated to 80 degrees, with the temperature being controlled and PID stabilised via an oven driver. Increasing this temperature allowed for ^{87}Rb deposited on the walls of the vapor cell to be excited and result in higher population density of ^{87}Rb atoms within the vapor.

Similar to the 795nm single photon spectroscopy, the Pound-Drever Hall technique was used to obtain a spectroscopy trace for the 762nm transition of ^{87}Rb . The frequency modulation was performed via an EOM to add sidebands to the carrier frequency and the 762nm beam after passing through the vapor cell was collected by a transimpedance amplifier, where the resulting signal is processed into a spectroscopy signal as given in Figure 25.

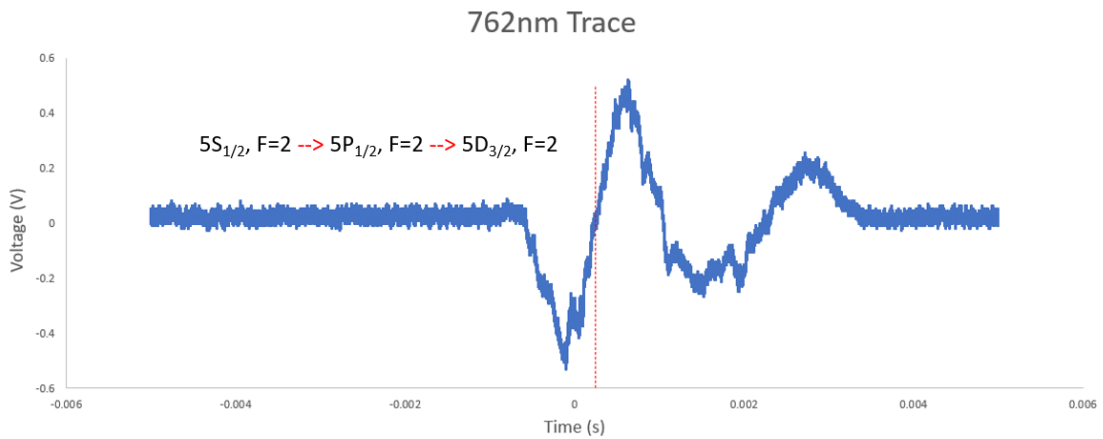


Figure 25: Error signal trace at 762nm regime for ^{87}Rb . Red vertical line represents a 762nm frequency that matches the $5P_{1/2}, F=2 \rightarrow 5D_{3/2}, F=2$ transition that a laser needs to be locked to for Six-Wave Mixing.

It is to be noted that frequency modulation via the EOM could be performed on both the 762nm beam and the 795nm beam entering the vapor cell. However, it was found that performing this frequency modulation on the 795nm beam resulted in a stronger error signal trace experimentally. The set-up via which this was achieved is as shown in Figure 26.

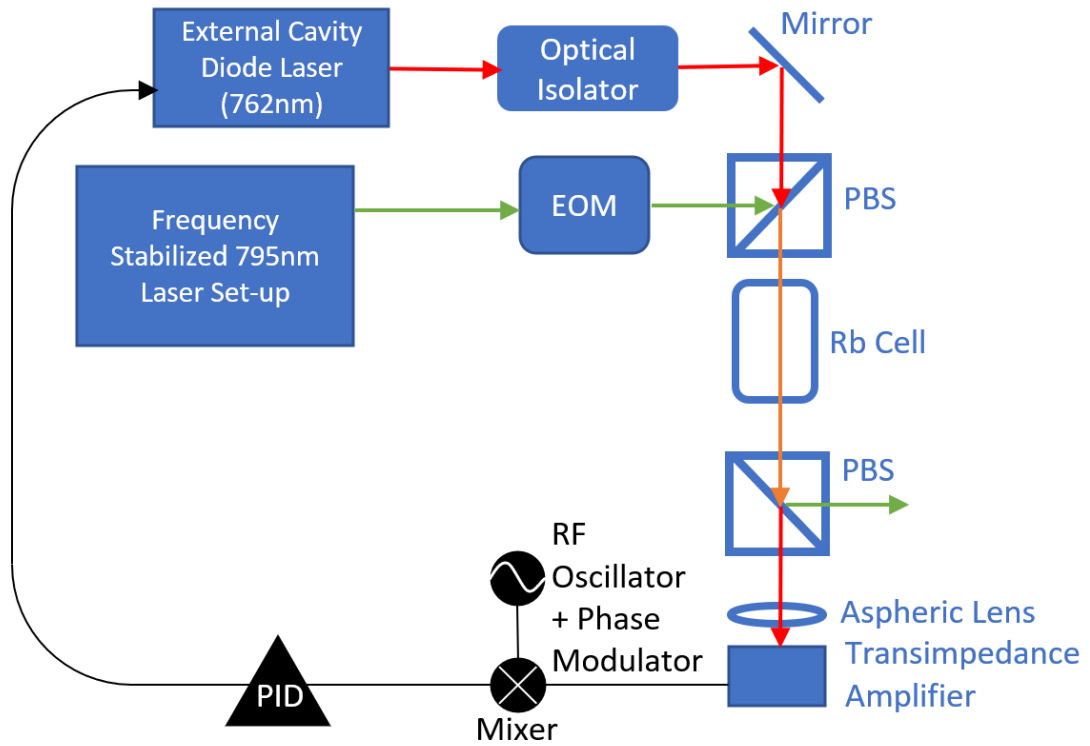


Figure 26: Schematic of Set-up used to perform Pound-Drever Hall locking on a 762nm External Cavity Diode Laser via 2-photon Rubidium. A 795nm laser locked to an ^{87}Rb transition was used to prepare photons at a higher excited state for the 762nm laser to perform spectroscopy. EOM: Electro-Optical Modulator, PBS: Polarising Beam Splitter, QWP: Quarter Wave Plate, Rb Cell: ^{87}Rb vapor cell. Refer to Figure 4 for schematic of ECDL

Another interesting phenomenon that was observed was fluorescence within the vapor cell when performing two-photon Rubidium spectroscopy, as shown in Figure 27. This fluorescence was postulated to be a result of the de-excitation of the ^{87}Rb atoms that were excited by a 795nm and 762nm photon, resulting in the production and scattering of an infrared photon with wavelength 5036nm and a 421nm wavelength photon (blue light in visible spectrum) which brings the excited atom back to ground state.

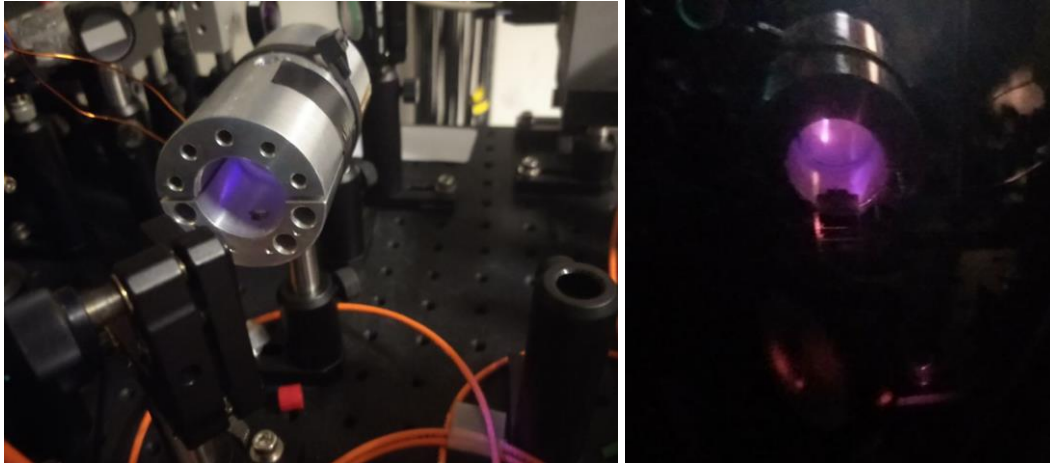


Figure 27: Iridescence observed from in ^{87}Rb . When 795nm and 762nm lasers are locked to atomic transition frequencies, the excited atoms de-excite back to ground state by emitting an infrared 5036nm photon and a blue 421nm photon, resulting in the blue light being observed from the vapor cell.

13 REFERENCES

- [1] T. Jennewein, C. Simon, G. Weihs, H. Weinfurter, and A. Zeilinger, “Quantum Cryptography with Entangled Photons,” *Phys. Rev. Lett.*, vol. 84, no. 20, pp. 4729–4732, May 2000, doi: 10.1103/PhysRevLett.84.4729.
- [2] A. Karlsson and M. Bourennane, “Quantum teleportation using three-particle entanglement,” *Phys. Rev. A*, vol. 58, no. 6, pp. 4394–4400, Dec. 1998, doi: 10.1103/PhysRevA.58.4394.
- [3] J. Preskill, “Quantum computing and the entanglement frontier,” *ArXiv12035813 Cond-Mat Physicsquant-Ph*, Nov. 2012, Accessed: Jan. 03, 2022. [Online]. Available: <http://arxiv.org/abs/1203.5813>
- [4] J. Persson, T. Aichele, V. Zwiller, L. Samuelson, and O. Benson, “Three-photon cascade from single self-assembled InP quantum dots,” *Phys. Rev. B*, vol. 69, no. 23, p. 233314, Jun. 2004, doi: 10.1103/PhysRevB.69.233314.
- [5] J. Douady and B. Boulanger, “Experimental demonstration of a pure third-order optical parametric downconversion process,” *Opt. Lett.*, vol. 29, no. 23, p. 2794, Dec. 2004, doi: 10.1364/OL.29.002794.
- [6] T. E. Keller, M. H. Rubin, Y. Shih, and L.-A. Wu, “Theory of the three-photon entangled state,” *Phys. Rev. A*, vol. 57, no. 3, pp. 2076–2079, Mar. 1998, doi: 10.1103/PhysRevA.57.2076.
- [7] M. Corona, K. Garay-Palmett, and A. B. U’Ren, “Third-order spontaneous parametric down-conversion in thin optical fibers as a photon-triplet source,” *Phys. Rev. A*, vol. 84, no. 3, p. 033823, Sep. 2011, doi: 10.1103/PhysRevA.84.033823.
- [8] M. G. Moebius *et al.*, “Efficient photon triplet generation in integrated nanophotonic waveguides,” *Opt. Express*, vol. 24, no. 9, p. 9932, May 2016, doi: 10.1364/OE.24.009932.
- [9] H. Hübel, D. R. Hamel, A. Fedrizzi, S. Ramelow, K. J. Resch, and T. Jennewein, “Direct generation of photon triplets using cascaded photon-pair sources,” *Nature*, vol. 466, no. 7306, pp. 601–603, Jul. 2010, doi: 10.1038/nature09175.
- [10] D. C. Burnham and D. L. Weinberg, “Observation of Simultaneity in Parametric Production of Optical Photon Pairs,” *Phys. Rev. Lett.*, vol. 25, no. 2, pp. 84–87, Jul. 1970, doi: 10.1103/PhysRevLett.25.84.
- [11] P. G. Kwiat, K. Mattle, H. Weinfurter, A. Zeilinger, A. V. Sergienko, and Y. Shih, “New High-Intensity Source of Polarization-Entangled Photon Pairs,” *Phys. Rev. Lett.*, vol. 75, no. 24, pp. 4337–4341, Dec. 1995, doi: 10.1103/PhysRevLett.75.4337.
- [12] C. Kurtsiefer, M. Oberparleiter, and H. Weinfurter, “High-efficiency entangled photon pair collection in type-II parametric fluorescence,” *Phys. Rev. A*, vol. 64, no. 2, p. 023802, Jul. 2001, doi: 10.1103/PhysRevA.64.023802.
- [13] T. Kim, M. Fiorentino, and F. N. C. Wong, “Phase-stable source of polarization-entangled photons using a polarization Sagnac interferometer,” *Phys. Rev. A*, vol. 73, no. 1, p. 012316, Jan. 2006, doi: 10.1103/PhysRevA.73.012316.
- [14] A. Haase, N. Piro, J. Eschner, and M. W. Mitchell, “Tunable narrowband entangled photon pair source for resonant single-photon single-atom interaction,” *Opt. Lett.*, vol. 34, no. 1, p. 55, Jan. 2009, doi: 10.1364/OL.34.000055.
- [15] A. Cerè, V. Parigi, M. Abad, F. Wolfgramm, A. Predojević, and M. W. Mitchell, “Narrowband tunable filter based on velocity-selective optical pumping in an atomic vapor,” *Opt. Lett.*, vol. 34, no. 7, p. 1012, Apr. 2009, doi: 10.1364/OL.34.001012.

- [16] M. Steiner, V. Leong, M. A. Seidler, A. Cerè, and C. Kurtsiefer, “Photon bandwidth dependence of light-matter interaction,” *Opt. Express*, vol. 25, no. 6, p. 6294, Mar. 2017, doi: 10.1364/OE.25.006294.
- [17] B. Srivathsan, G. K. Gulati, B. Chng, G. Maslennikov, D. Matsukevich, and C. Kurtsiefer, “Narrow Band Source of Transform-Limited Photon Pairs via Four-Wave Mixing in a Cold Atomic Ensemble,” *Phys. Rev. Lett.*, vol. 111, no. 12, p. 123602, Sep. 2013, doi: 10.1103/PhysRevLett.111.123602.
- [18] R. W. Boyd, *Nonlinear optics*, 3rd ed. Amsterdam ; Boston: Academic Press, 2008.
- [19] M. Rambach, A. Nikolova, T. J. Weinhold, and A. G. White, “Sub-megahertz linewidth single photon source,” *APL Photonics*, vol. 1, no. 9, p. 096101, Dec. 2016, doi: 10.1063/1.4966915.
- [20] G. Lin, P.-Y. Su, and H.-C. Cheng, “Low threshold current and widely tunable external cavity lasers with chirped multilayer InAs/InGaAs/GaAs quantum-dot structure,” *Opt. Express*, vol. 20, no. 4, p. 3941, Feb. 2012, doi: 10.1364/OE.20.003941.
- [21] THORLABS, “808 nm Fabry-Perot Laser Diode, 100 mW LD808-SA100.” Accessed: Jan. 03, 2022. [Online]. Available: <https://www.thorlabs.com/drawings/7b3e76faf5d81ce-3F4B600F-C08A-109D-B52459176788AE0C/LD808-SA100-SpecSheet.pdf>
- [22] Tyll Hertsens, “Measuring diode laser characteristics: diode lasers approach ubiquity, but they still can be frustrating to work with.” Reed Business Information, Inc. (US), Feb. 1989. [Online]. Available: https://www.newport.com/medias/sys_master/images/images/he9/hd7/8797049520158/AN05-Laser-Diode-Characteristics-Overview.pdf
- [23] P. W. Milonni and J. H. Eberly, *Lasers*. New York: Wiley, 1988.
- [24] G. Gagliardi and H.-P. Looock, *Cavity-enhanced spectroscopy and sensing*. Heidelberg: Springer, 2014.
- [25] Adrian Nugraha Utama, “Elongated cloud of cold 87rb atoms: Towards a brighter source of narrowband photon pairs,” National University Singapore, Centre for Quantum Technologies, 2016.
- [26] Bharath Srivathsan, “HERALDED SINGLE PHOTONS FOR EFFICIENT INTERACTION WITH SINGLE ATOMS,” National University Singapore, Centre for Quantum Technologies, 2014.